scientific reports



OPEN

Comparative analysis of traditional and Gaussian Analytical Hierarchy Process (AHP) methods for landslide susceptibility assessment

Rômulo Marques-Carvalho^{1⊠}, André Carlos Ponce de Leon Ferreira de Carvalho¹, Elton Vicente Escobar-Silva², Renata Pacheco Quevedo^{3⊠}, Cláudia Maria de Almeida⁴ & Marcos Santos⁵

This study applies the Gaussian Analytical Hierarchy Process (Gaussian AHP) to landslide susceptibility mapping and demonstrates its superior methodological rigor and predictive performance relative to the traditional AHP method. Susceptibility maps produced by Gaussian AHP allocated 26.31% of the study area to the very high susceptibility class, outperforming the traditional AHP's estimated share (23.52%), and achieved a more balanced distribution across all five classes. Validation against a high resolution inventory of 97,742 landslide samples collected during the February 2023 São Sebastião event—divided into 70% training and 30% validation subsets—vielded improved metrics: ROC area under the curve of 0.6360 versus 0.6220; overall accuracy of 0.6364 versus 0.6229, balanced accuracy of 0.6356 versus 0.6221; and sensitivity of 0.3585 versus 0.3116, for the Gaussian and traditional AHP methods respectively. An uncertainty analysis quantified a 56.16% disagreement between the two methods, revealing that Gaussian AHP reduced classification ambiguity in critical classes. A complementary density-based assessment, comparing observed landslide crown points and scar polygons against susceptibility class areas, showed that Gaussian AHP produced a gradual, coherent increase in normalized landslide density from very low to very high susceptibility, whereas traditional AHP displayed sharp breaks in intermediate classes. These findings confirm that Gaussian AHP enhances objectivity, spatial coherence, and operational reliability, better aligning high density landslide clusters with the highest susceptibility zones. By leveraging statistical weighting, Gaussian AHP streamlines data preprocessing and reduces the need for expert calibration, making it well suited for assessments in data rich environments. The statistical weighting procedure facilitates the integration of diverse geospatial datasets and supports robust, reproducible multicriteria decision analysis. Its integration with accurate machine learning-derived land use/land cover data and refined climate data is recommended to further improve predictive accuracy and support proactive landslide risk management strategies. The proposed approach can additionally meet operational purposes, provided that near real-time climate data, updated geospatial databases, and massive computing resources are available.

Since the early 21^{st} century, landslides have increasingly been recognized as a significant threat to human settlements, particularly in urban areas experiencing heavy rainfall¹. This increased risk is largely attributed to the growing vulnerability of fast urbanization, which transforms landscapes and disrupts drainage systems, increasing the susceptibility to such geological hazards². In 2024, this threat materialized in various regions worldwide, including Nepal³, the United States - where Hurricane Helena triggered widespread landslides⁴ – and Taiwan⁵. In South America, more than 30% of recorded landslides occurred in Brazil⁶, predominantly impacting the South and Southeast regions⁷.

¹Institute of Mathematics and Computer Science, University of São Paulo, São Carlos 13566-590, Brazil. ²National Center for Monitoring and Early Warning of Natural Disasters, São José dos Campos 12247-016, Brazil. ³Present address: ENGAGE Research Group, Department of Geography and Regional Research, University of Vienna, Vienna 1010, Austria. ⁴National Institute for Space Research, São José dos Campos 12227-010, Brazil. ⁵Department of Science and Technology, Military Institute of Engineering, Rio de Janeiro 22290-270, Brazil. [™]email: romulomarques@usp.br; renata.quevedo@univie.ac.at

Although landslides are natural phenomena triggered by extreme precipitation events, seismic activity, volcanic eruptions, wildfires and other environmental processes⁸, besides anthropogenic activities are affecting slope stability⁶. For instance, deforestation, construction works, and abandonment of farming areas affect hillslope stability, changing natural stress state and force equilibrium⁹. As a result, landslides have become a pressing issue in urban policy development, requiring their integration into comprehensive strategies to mitigate climate change¹⁰.

The significant impacts of landslide events have led to the development of numerous methods for assessing landslide susceptibility¹¹⁻¹³. These methodologies follow diverse approaches, such as heuristic, physically-based, and statistical modeling techniques¹⁴. Among the semi-quantitative models, ¹⁵ used the Analytical Hierarchy Process (AHP) to assess landslide susceptibility. One commonly used approach relies on the multi-criteria decision analysis, off which AHP is particularly prominent¹⁶, especially in Brazilian research¹⁷. This method effectively identifies and prioritizes the factors contributing to landslide occurrences¹⁸, creating a pairwise comparison matrix that weights each factor based on its relative influence on landslide risk. This mathematical framework serves as a structured decision-making tool that organizes complex problems into a hierarchy of criteria, sub-criteria, and alternatives¹⁹. Researchers perform pairwise comparisons to evaluate the relative importance of elements within each hierarchy level. This comparison results in a matrix from which the principal eigenvector is derived, representing the normalized priorities of each component. Furthermore, this approach integrates quantitative data with expert judgment, supporting nuanced decisions in complex scenarios²⁰, such as evaluating landslide susceptibility.

Despite considerable advancements in deep learning models applied in various fields over the past decade²¹, the AHP technique continues to hold significance in the literature on landslides^{22,23}. Huang et al. (2020) conducted a comparative study of AHP, statistical, and machine learning-based models for predicting and mapping landslide susceptibility in Shicheng, China²⁴. Sonker, Tripathi, and Singh (2021) combined remote sensing data, geographical information system (GIS), and AHP to create landslide susceptibility maps for Sikkim Himalaya, India²⁵. Panchal and Shrivastava (2022)²⁶ used AHP to evaluate landslide hazards along a highway in India. Zhou et al. (2023) applied the method to assess landslide disaster susceptibility at a photovoltaic power generation construction site in Yunxian County, China²⁷. Kucuker (2024) evaluated the landslide risk potential for forest roads in Trabzon, Turkey, using AHP²⁸. Liu, Shao, and Shao (2024) applied AHP for landslide susceptibility zonation in the Greater Xi'an Region, China²⁹. Ou, Huang, and Cao (2024) introduced multiple rainfall indexes to optimize a landslide model based on AHP³⁰. Gulbet and Getahun (2024) compared susceptibility mapping techniques using frequency ratio and the AHP method in Awabel Woreda, Ethiopia³¹. Mengstie et al. (2024) integrated remote sensing and GIS data to assess landslide susceptibility in Addi Arkay, Ethiopia, using AHP³². Singh et al. (2024) employed the method for detailed landslide susceptibility index (LSI) mapping from remotely sensed data in the Beas River basin, Himalaya³³. Dahmani et al. (2024) analyzed landslide dynamics in the Chefchaouen province, Morocco, adopting a multi-criteria spatial approach and GIS, using AHP³⁴. Kshetrimayum, Ramesh, and Goyal (2024) explored various approaches, including AHP, for zonation mapping of landslide susceptibility in Manipur, India³⁵

However, the AHP method has significant limitations³⁶, such as its dependence on subjective expert evaluations, which can introduce biases and complicate the analysis of processes involving multiple criteria. To address these challenges, the Analytical Hierarchy Process – Gaussian (Gaussian AHP) approach³⁷ was developed, replacing traditional pairwise comparisons with a framework based on statistical measures, and employing the normal distribution to build the comparison matrix. This technique employs the mean (as an estimate) and the standard deviation (as a measure of uncertainty) of the relative importance of each variable, incorporating the Gaussian factor as a mechanism for ranking the alternatives. By reducing the subjectivity inherent in judgments and enabling the analysis of many criteria, Gaussian AHP provides greater rigor and precision, as shown by sensitivity analyses that bolster the reliability of the results³⁸. In this context, this study aims to evaluate the performance of the Gaussian AHP method in integrating GIS and remote sensing data for landslide susceptibility assessment compared to the traditional AHP approach. This innovative methodology was tested in a case study in Brazil, demonstrating its potential to improve precision in multi-criteria analysis applied to susceptibility assessment.

Materials and methods Study area

The landslide susceptibility map of Brazil⁷, published by the Brazilian Institute of Geography and Statistics (IBGE) in 2019, revealed that cities in the southeastern and southern regions are more prone to this hazard than those in other regions. This case involves the municipality of São Sebastião (Fig. 1), a coastal city in the state of São Paulo, known for its landscape dominated by mountains, escarpments, and high hills.

Among the São Paulo municipalities with extremely high vulnerability to natural disasters related to landslides—i.e., the fragility degree to which the municipality is exposed — São Sebastião ranks 7^{th} out of 26 municipalities⁴². Furthermore, when calculating the vulnerability index to natural disasters related to landslides (*Îndice de Vulnerabilidade aos Desastres Naturais relacionados com Deslizamento de Terra - IVDDT*), the author identified São Sebastião as the most vulnerable municipality among those classified as having extremely high vulnerability to landslides. This vulnerability was confirmed during the landslide event of February 2023, triggered by intense rainfall, which resulted in significant socioeconomic damage and casualties. This event has been widely investigated in various studies^{41,43–47} due to its relevance in understanding the determinants of socio-environmental vulnerability and in formulating mitigation and adaptation strategies for disasters associated with landslides.

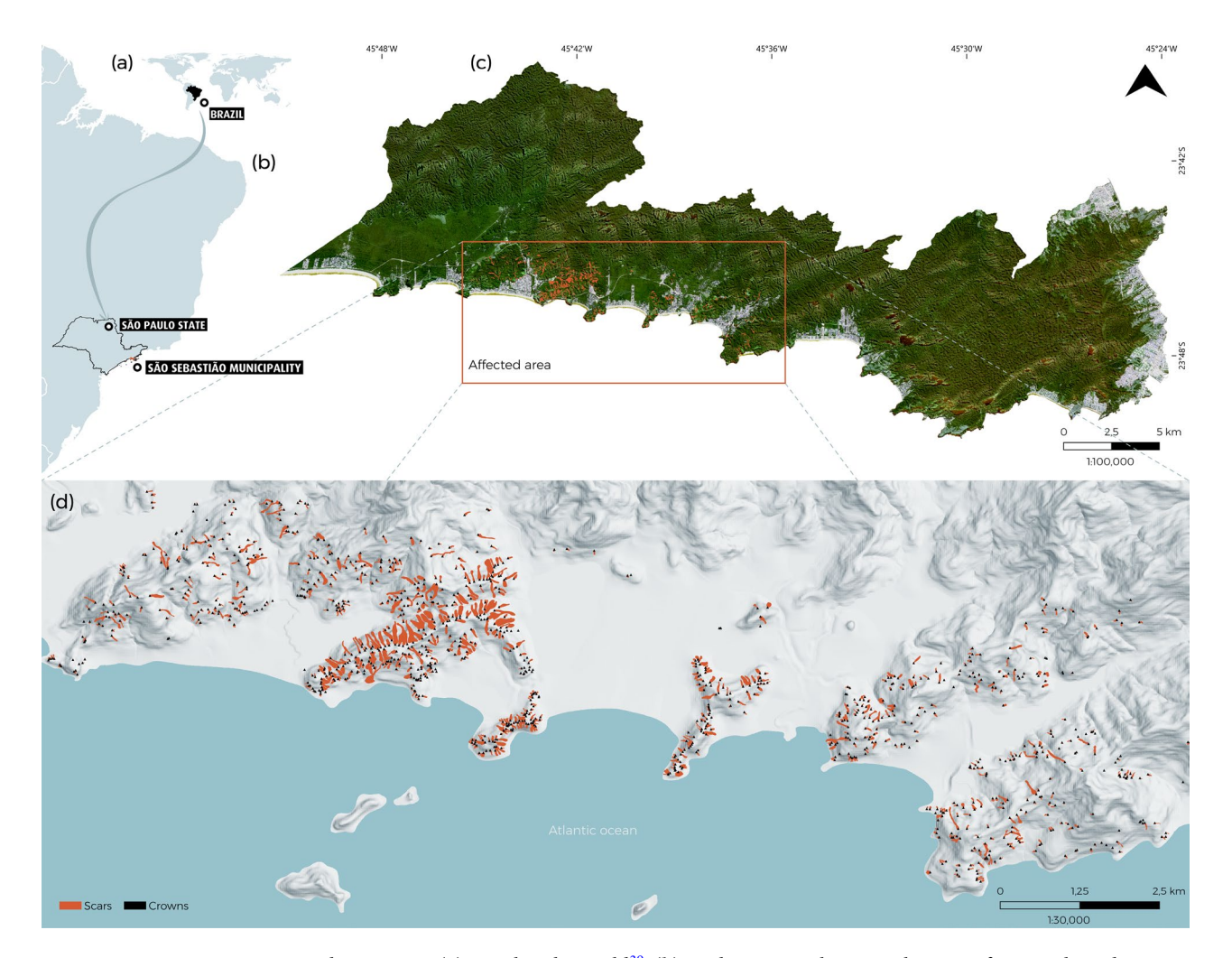


Fig. 1. Study area map: (a) Brazil in the world³⁹, (b) Study area in relation to the state of São Paulo and Brazil³⁹, (c) Sentinel-2 true color composite⁴⁰ from February 22, 2023, of the study area, (d) Area affected by landslides during the February 2023 disaster⁴¹. (The data for Fig. a and b is sourced from an IBGE public repository availabe at https://www.ibge.gov.br/geociencias/downloads-geociencias.html. The data for Fig. c is sourced from a public Sentinel-2 image available at https://apps.sentinel-hub.com/eo-browser/. The data for Fig. d is sourced from a public repository available at https://zenodo.org/records/11120078. The processing software used is QGIS version 3.40.8, available at https://qgis.org/en/site/).

Methods

The methodology of this study was structured into four subsections: data acquisition and generation, AHP and Gaussian AHP analyses, susceptibility map generation, and model validation.

Data acquisition

Since there is no universal consensus in the literature regarding the selection of variables for assessing landslide susceptibility⁴⁸, many studies explore different landslide conditioning factors⁹. For instance, recent studies highlight the significance of factors such as morphometric factors, which include slope, aspect, terrain curvature, and elevation, in landslide susceptibility modeling^{49,50}. Based on these findings, we considered a total of 16 landslide conditioning factors (Table 1) to model susceptibility in São Sebastiao municipality.

Before using the DTM to derive morphometric factors, preprocessing was conducted to identify and fill in pixels with missing information within the study area, thus to guarantee a hydrological corrected DTM. For this purpose, the algorithm proposed by Wang and Liu (2006)⁸³ was employed, which identifies and fills surface depressions in digital elevation models. This method ensures the topographic continuity needed for more accurate morphometric analyses. Subsequently, the slope, relative slope position, aspect, curvature (plan and profile), convergence index, and topographic wetness index⁸⁴ variables were derived using the Basic Terrain Analysis tool, while the Terrain Ruggedness Index was generated using the Terrain Ruggedness Index tool⁸⁵, both implemented in the SAGA GIS software. The proximity factors (distance to rivers and distance to roads) represent the distance between the center of each pixel and the center of the nearest pixel, generated using the GDAL proximity tool⁸⁶. The land cover map corresponds to a classification of a CBERS-4A satellite image, employing data mining, image segmentation, and the random forest algorithm⁷¹. The other variables were

Variables	Definition	Source
Slope	The measure of surface inclination, typically expressed in degrees or percentages. It is derived from the DTM and is used to classify topographic parameters and identify areas with a higher frequency of landslides, playing a crucial role in assessing terrain stability and landslide risks 1-53.	DTM ⁵⁴
Aspect	The azimuthal orientation of the slope influences the incidence of exogenous factors such as sunlight, wind, and rainfall. This variable directly affects weathering, vegetation cover, and the hydrological dynamics of the slope, conditioning its susceptibility to mass movements ⁵⁵ .	DTM ⁵⁴
Elevation	This represents the altitude of a point in relation to sea level (topographic elevation) or the difference in altitude between relief features (relative elevation). This variable affects water pressure in the soil, surface runoff, and gravitational potential energy, consequently affecting slope stability and the likelihood of landslides ⁵⁶ .	DTM ⁵⁴
Plan curvature	This refers to the rate of change of the flow direction $(\varphi + \pi)$ along the direction of the vector $\left(\frac{\nabla^{\perp} f}{S}\right)$, i.e., following a contour line. In the context of landslides, this curvature indicates how the terrain curves laterally, affecting the dispersion of surface flow and soil stability ⁵⁶ .	DTM ⁵⁴
Profile curvature	The rate of change of the surface slope along the direction of the unit vector $(-\nabla/S)$, i.e., following the flow line in a downward direction. In the context of landslides, this measure indicates how the terrain curves towards the flow, affecting the accumulation and dynamics of water and sediment ⁵⁷ .	DTM ⁵⁴
Convergence Index	This metric assesses the slope curvature by calculating the average of the slope directions of neighboring pixels in relation to the direction of the central pixel. In the context of landslides, negative values indicate convergent areas favoring the accumulation of water and materials, while positive values represent divergent areas, where surface flow is dispersed, influencing the potential for soil instability ^{58–60} .	DTM ⁵⁴
Relative slope position	This represents the ratio the slope height to the elevation difference, measured from the ridge or summit to the valley floor, and describes the topographical position of the terrain. This variable is crucial for landslide analysis, as it helps to identify areas of greater susceptibility based on the terrain's relative position, influencing processes such as water accumulation, sediment dynamics, and soil stability ^{61,62} .	DTM ⁵⁴
Terrain Ruggedness Index (TRI)	This measures of the variation in elevation between a cell and its neighbors in a DTM, reflecting topographic roughness. This index is crucial for landslide analysis, as areas with greater roughness tend to have a higher risk of instability ^{63,64} .	DTM ⁵⁴
Topographic Wetness Index (TWI)	This quantifies soil moisture variation by integrating upstream water supply and downstream runoff in a DTM. It combines the slope gradient with the specific catchment area. TWI is crucial for landslide analysis, as areas with higher soil moisture face a greater risk of instability 65,66.	DTM ⁵⁴
Distance to rivers	This refers to the Euclidean (straight-line) distance to water bodies. It is a critical factor for landslide analysis, as proximity to water bodies can increase the risk of slope erosion and soil saturation. Most landslides occur in areas close to rivers, particularly within a 200-meter radius. This variable should be incorporated into risk models to accurately identify high-risk zones ^{67,68} .	IBGE ⁶⁹
Land cover	The physical characteristics of the Earth's surface, such as vegetation, water bodies, and built structures. It describes the natural and human-made features that occupy a specific area. Land cover plays an important role in landslide analysis, as it influences soil stability, water retention, and slope stability, helping to identify areas at higher risk for landslides ^{9,70} .	Marques- Carvalho et al. (2025) ⁷¹
Lithology	This refers to physical and mineralogical characteristics of sediments and rock types within the Earth's stratigraphy. It is crucial in landslide studies, as it influences spatial variation in landslide prevalence, type, and depth by affecting properties such as porosity, permeability, and water saturation, which determine soil and rock stability ^{72,73} .	SGB (2017) ⁷⁴
Geomorphology	Land relief is the shape and structure of the earth's surface resulting from geomorphological processes involving endogenous forces (such as faults and folds) and exogenous forces (such as climate, gravity, water, wind and ice), which are responsible for the continuous shaping and transformation of the terrain 75,76.	SGB (2017) ⁷⁴
Pedology	This influences slope stability and is determined by texture and clay content. Clay soils, such as andosols, latosols, and organosols, tend to retain more water, increasing the risk of landslides, whereas sandy soils, such as regosols, are more permeable, reducing this risk ^{77,78} .	SGB (2017) ⁷⁴
Rainfall	Heavy rainfall alters the dynamics of surface and groundwater, reducing soil stability and triggering landslides. This occurs due to increased soil saturation and a decrease in particle cohesion ^{79,80} .	SGB (2017) ⁷⁴
Distance to roads	Influences landslide susceptibility due to soil disturbances caused by cut-and-fill works, changes in drainage, and unplanned human activities. Traffic vibrations can weaken slope materials, compact the soil, and increase the risk of instability ⁸¹ .	DataGEO (2013) ⁸²

Table 1. Predictor variables.

sourced directly from the Geological Survey of Brazil (SGB) geospatial database, whereby the vectors underwent a rasterization process. Fig. 2 presents all the variables used, highlighting their interdependence with the occurrence of the most recent landslide event in 2023.

The validation of the susceptibility map was fully supported by the landslide inventory compiled by Coelho et al. (2024)⁴¹ for the February 2023 event in São Sebastião, used here without any reinterpretation of the original data. The inventory was created through manual digitization of 10 cm-resolution aerial imagery from the São Paulo State Spatial Data Infrastructure (*Infraestrutura de Dados Espaciais de São Paulo - IDE-SP*), supplemented by historical orthophotos from Google Earth and PlanetScope scenes. The dataset includes 983 landslide crown points — locations indicating the undisturbed material adjacent to the head of scars — and 1,070 landslide scar polygons outlining the displaced material area. Each feature contains planar geometric attributes (area, perimeter, length, and width) and volumetric estimates based on average failure depth (0.5 m to 2.8 m), along with geological context and land-cover information. It is worth mentioning that another inventory of landslides crowns and scars was recently released for the 2023 extreme event in São Sebastião⁸⁷. Nevertheless, we adopted the one produced by⁴¹, for it was grounded on extensive field work, and hence, presents a greater level of detail and comprehensiveness.

To characterize crowns and scars in detail, the authors extracted geomorphometric parameters — elevation (3.00 m to 458.10 m), slope (0.82° to 63.08°), aspect, and profile curvature — sampled at crown locations. The scars show a strongly right-skewed distribution of polygon area (mostly under 5,000 m²), with shapes ranging from small triangular features to large bodies exceeding tens of thousands of square meters. Crowns, represented as points at the start of each landslide, mainly cluster between 50 m and 100 m elevation, with slope values peaking around 30°.

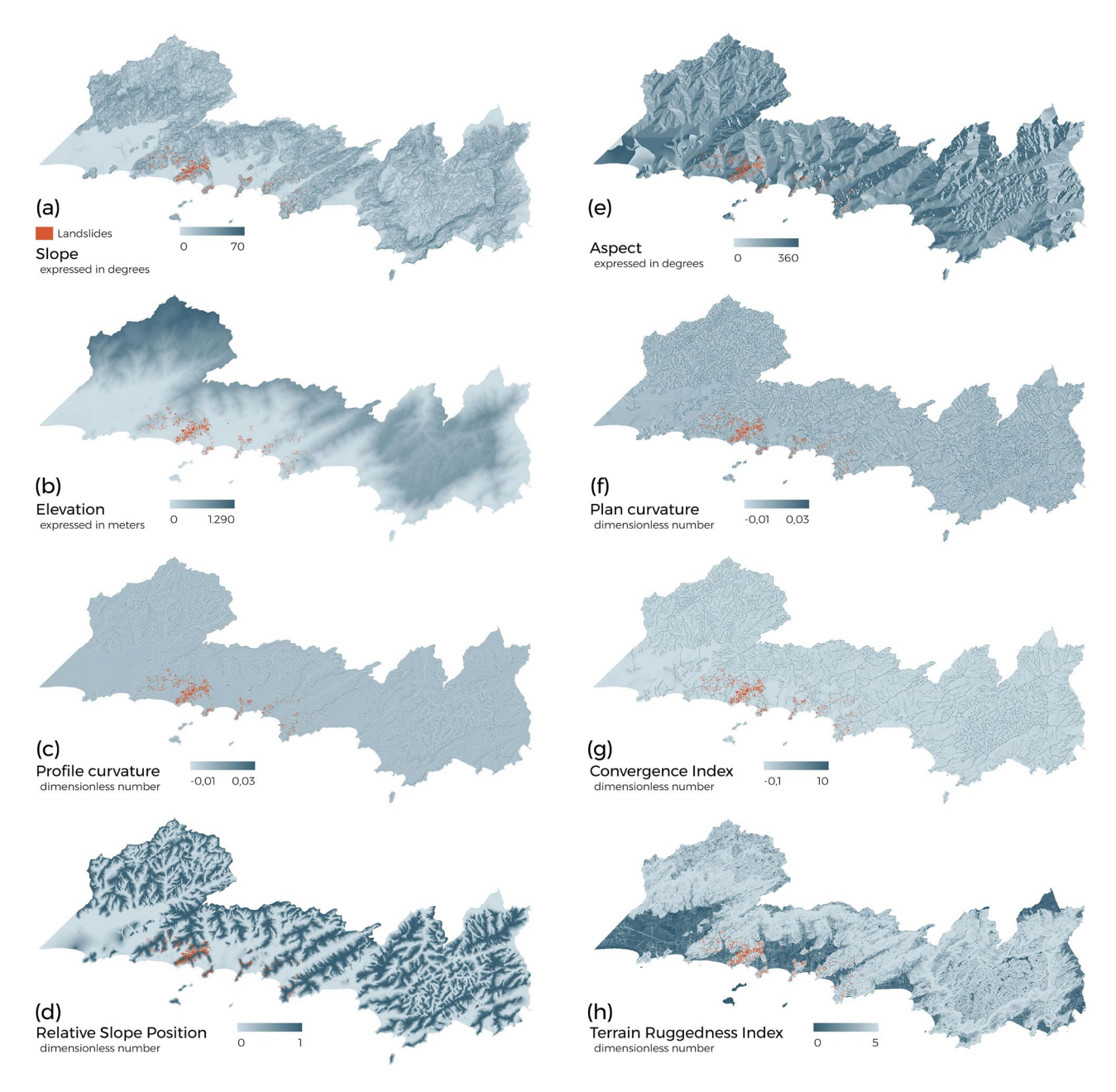


Fig. 2. Spatial distribution of landslide occurrences superimposed on each explanatory variable layer: (a) Slope, (b) Elevation, (c) Profile Curvature, (d) Relative Slope Position, (e) Aspect, (f) Plan Curvature, (g) Convergence Index, (h) Terrain Ruggedness Index. (i) Topographic Wetness Index, (j) Land Cover, (k) Geomorphology, (l) Average Annual Precipitation, (m) Distance to Rivers, (n) Lithology, (o) Pedology, (p) Distance to Roads.

Analytical hierarchy process method

The AHP is a multi-criteria analysis approach introduced by Saaty (1977)¹⁹. It offers a structured approach for evaluating complex decision problems by performing pairwise comparisons to determine the relative importance of criteria and alternatives, aiming to assign weights that reflect their hierarchical significance. AHP employs Saaty's 1-9 Scale of Pairwise Comparisons¹⁹, where a value of 1 denotes equal importance and 9 indicates extreme importance, with intermediate values representing gradual levels of relative importance. This scale allows experts to assign numerical values based on their domain knowledge of the relative importance of one variable compared to another in explaining the analyzed phenomenon. Saaty's scale simplifies the judgment process by providing clear definitions for each level of comparison (Table 2).

The traditional \overline{AHP} method is based on a pairwise matrix and was implemented in R language within the RStudio environment (version 4.2.3, 2023-03-15 UCRT)⁸⁸, using the *raster*, *sp*, and magrittr packages for spatial data processing. The pairwise matrix (Eq. 1) must be developed based on reciprocal logic, i.e., if variable x is more important than variable y, the relationship of importance between x and y must be symmetrically reflected,

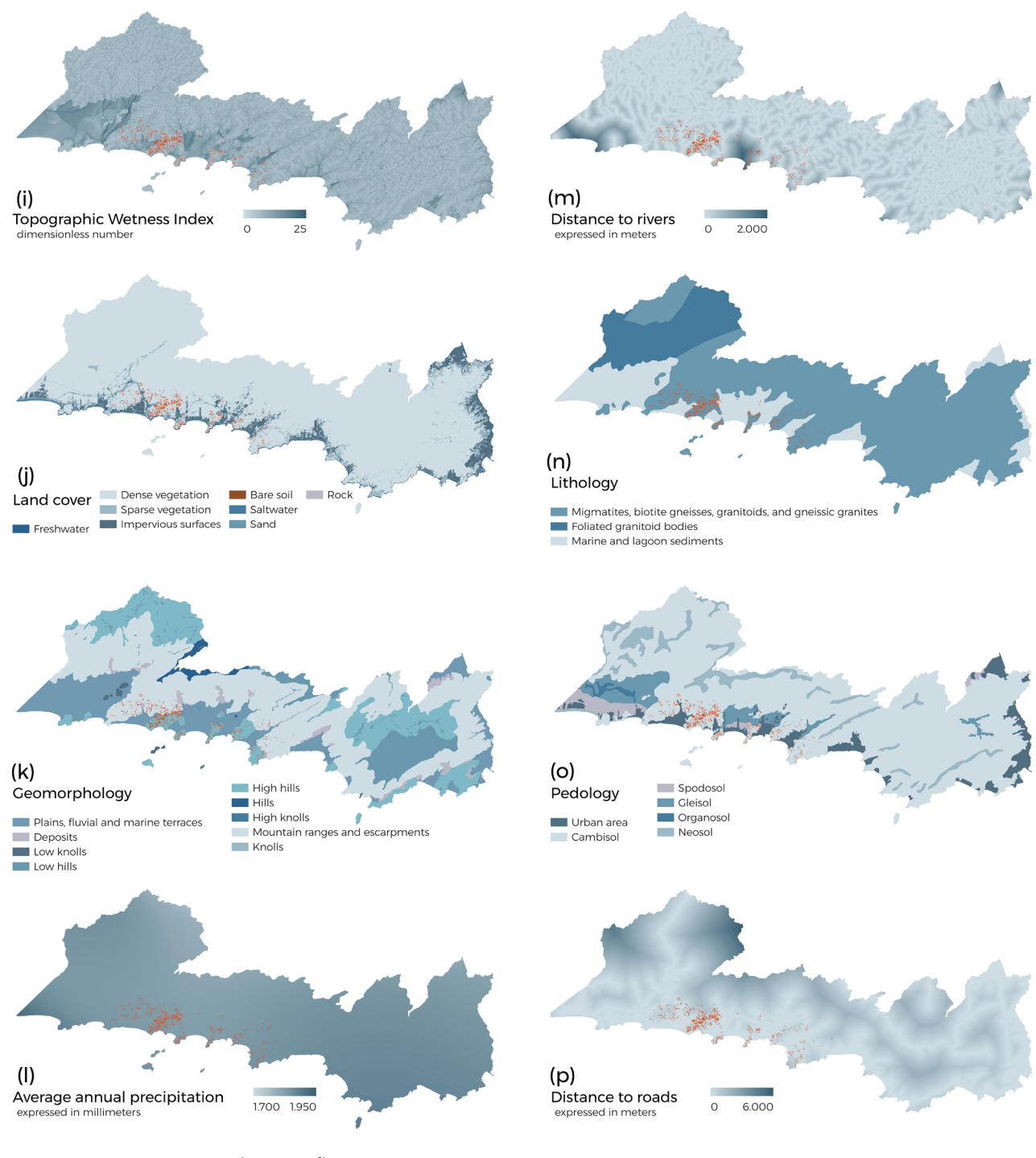


Fig. 2. (continued)

that is, the comparison of y relative to x must be inverted (x > y implies y < x). Furthermore, if variable z is more important than y, but not necessarily more important than x, reciprocal consistency must be maintained to ensure that the comparison hierarchy remains logical and coherent x. This systematization is essential for ensuring that the relationships assigned in the pairwise matrix are consistent, allowing the weight calculations to be valid and faithfully represent the decision maker's preferences. The weights of the traditional AHP method were defined according to a consensus reached among experts from the field of environmental management, disaster monitoring and management, geography, and urban planning.

Intensity of importance	Definition	Explanation
1	Equal importance	Two activities contribute equally to the objective.
3	Weak importance of one over another	Experience and judgment slightly favor one activity over another.
5	Essential or strong importance	Experience and judgment strongly favor one activity over another.
7	Demonstrated importance	An activity is strongly favored and its dominance is demonstrated in practice.
9	Absolute importance	The evidence favoring one activity over another is of the highest possible order of affirmation.
2,4,6,8	Intermediate values between the two adjacent judgments	When compromise is needed.
Reciprocals	Inverse comparison	If activity i has one of the above nonzero numbers assigned to it when compared with activity j , then j has the reciprocal value when compared with i .

Table 2. Saaty's 1-9 Scale of Pairwise Comparisons 19.

$$M = \begin{bmatrix} 1 & a_{12} & a_{13} & \cdots & a_{1n} \\ a_{21} & 1 & a_{23} & \cdots & a_{2n} \\ a_{31} & a_{32} & 1 & \cdots & a_{3n} \\ \vdots & \vdots & \vdots & \ddots & \vdots \\ a_{n1} & a_{n2} & \cdots & \cdots & 1 \end{bmatrix}$$
 (1)

The matrix was normalized according to Eq. 2 to enable a proper comparison between the criteria. This normalization process converts the original values of the comparison matrix into relative proportions, ensuring that the weights assigned to each criterion are consistent and comparable. Normalization is performed by dividing each element of the matrix by the sum of its respective column, thereby adjusting the values of each criterion to a common scale.

$$n_{ij} = \frac{a_{ij}}{\sum a_{ij}} \tag{2}$$

where n_{ij} is the normalized importance of the criterion, ranging between 0 and 1; a_{ij} is the value assigned to the importance of the criterion; $\sum a_{ij}$ is the sum of the importance values of the criteria by column.

Finally, the analysis of consistency was performed using the consistency ratio (CR), which is derived from Eq. 3. This index assesses the consistency of comparisons made in a pairwise matrix, which evaluates the relative importance of different criteria or alternatives or alternatives. The CR is calculated by taking the ratio between the consistency index (CI) of matrix and the random consistency index (RI), which varies depending on the matrix size. When the CR is less than 0.1, it indicates that the comparisons are consistent, meaning there are no significant contradictions between them. If the CR is greater than 0.1, the comparisons should be reviewed, as this suggests inconsistencies that could compromise the analysis.

$$CR = \frac{\lambda_{\text{max}} - n}{n - 1} \cdot \frac{1}{RI} \tag{3}$$

where λ_{max} is the maximum eigenvalue of the pairwise matrix, n is the maximum number of factors, and RI is the random consistency index⁹¹.

Gaussian AHP method

The Gaussian AHP³⁷ offers a novel approach to the original AHP method by incorporating sensitivity analysis through the Gaussian factor. This methodology enables the determination of attribute weights based on quantitative inputs of the alternatives within their respective attributes without requiring pairwise comparisons of alternatives and criteria³⁷. This innovative approach has been widely applied in various studies in operational research and is used as an efficient tool for addressing complex decision-making challenges. By incorporating quantitative factors and sensitivity analysis, it proves particularly valuable in scenarios requiring technical rigor and methodological consistency. As a result, it has gained increasing recognition among experts in the field^{38,92-96}.

This method³⁷ was adapted for applications to geospatial data, following a series of key procedures. Initially, the input variables (raster data) were imported, and their minimum and maximum values were explicitly defined. This step ensures that only valid pixel values are considered, preserving the quality of the data used to build the decision matrix. For each raster layer, pixel values were extracted and stored in vectors. Moreover, dummy values were removed to avoid interference in subsequent calculations. Each extracted vector was then normalized by dividing each value by the sum of the vector, ensuring that the total sum equaled 1. Normalization is essential for standardizing the data, allowing all variables to be compared on the same scale. Subsequently, the mean of the normalized values for each variable was computed to capture the central tendency of the data for each variable (Eq. 4). The standard deviation of the normalized values was also calculated to assess the dispersion of the data around the mean, providing information on the variability of each variable (Eq. 5).

$$\mu_{\text{variable}} = \frac{1}{n} \sum_{i=1}^{n} \text{normalized pixel value}$$
 (4)

$$\sigma_{\text{variable}} = \sqrt{\frac{1}{n-1} \sum_{i=1}^{n} (\text{normalized pixel value} - \mu_{\text{variable}})^2}$$
 (5)

where n is the number of pixels in each raster.

The Gaussian factor for each variable quantifies its variability and is calculated by dividing the standard deviation by the mean (Eq. 6), which quantifies the variability of each variable. The Gaussian factors are then normalized (Eq. 7), ensuring that each variable contributes in a balanced manner to the final inference. The Gaussian AHP inference is obtained by weighting the input rasters, following Eq. 8, with the normalized Gaussian factors, integrating all the variables into a single raster layer. Finally, the inference result is saved in a new raster file, facilitating geospatial analysis and visualization.

$$f_{\text{gaussian, variable}} = \frac{\sigma_{\text{variable}}}{\mu_{\text{variable}}}$$
 (6)

where

 $f_{\rm gaussian, \ variable}$ = Gaussian factor for each variable

 $\sigma_{\rm variable}$ = Standard deviation of the normalized values for the variable

 μ_{variable} = Mean of the normalized values for the variable

$$f_{\text{gaussian, normalized, variable}} = \frac{f_{\text{gaussian, variable}}}{\sum_{i=1}^{n} f_{\text{gaussian, variable}}}$$
 (7)

where

 $f_{
m gaussian,\ normalized,\ variable}$ = Normalized Gaussian factor for each variable

n = Total number of variables

i = Index of the variable in the summation

Inference_{AHP, Gaussian} =
$$\sum_{i=1}^{n} (\text{raster}_{i} \times f_{\text{gaussian, normalized, variable}_{i}})$$
(8)

where

Inference_{AHP, Gaussian} = Final Gaussian AHP inference

 $raster_i = Raster values of each variable$

 $f_{\rm gaussian,\ normalized,\ variable_i}$ = Normalized Gaussian factor for each variable i

The Gaussian AHP method was also implemented within the R Studio environment, using the same version adopted for the traditional method and employing the same spatial data processing packages. Initially, each raster layer (variables) was imported with the raster function, and its minimum and maximum values were adjusted by applying <code>setMinMax</code> to ensure consistency in internal metadata for validation. Then, pixel values were extracted with the values function, and NA (dummy) values were removed to avoid biases in the statistical analysis. Each pixel vector was normalized so that the sum of its elements equaled one. This step allowed for comparability across attributes with different units and scales.

For each normalized vector, the mean and standard deviation were calculated. The Gaussian factor for each variable was then defined as the ratio of the standard deviation to the mean, providing a quantitative measure of the spatial variability relative to central tendency. These Gaussian factors were normalized by the sum of all factors, yielding a set of weights that add up to one. The final Gaussian AHP output was produced by performing a weighted linear combination of the original raster layers, where each layer was multiplied by its corresponding normalized Gaussian weight. The resulting composite raster was assigned a UTM Zone 23S (WGS84) coordinate reference system and a spatial resolution of 5 m. This final product was exported in GeoTIFF format, enabling integration and visualization in standard GIS platforms, such as QGIS, in the particular case of this study.

Regarding variable types, the method applies the same statistical preprocessing to both continuous and categorical data. For nominal rasters (e.g., land use or lithology), class values are numerically encoded solely to facilitate computational processing. These numeric codes do not imply any inherent order or weighting. The weights are derived solely from the statistical relationship between the mean and standard deviation of normalized values, thus representing the intrinsic spatial variability of each layer. This approach ensures methodological rigor and supports the integration of diverse variables into a unified multi-criteria framework without introducing subjective or preconceived biases. Additionally, this approach allows future replications to use nominal variables without restrictions. Fig. 3 shows the flowchart of the methodological workflow used for implementing the Gaussian AHP model. The diagram illustrates each step of the process, from initially inputting raster variables to creating the final susceptibility map. Key steps include data normalization, calculation of Gaussian factors, assigning weights, and combining layers with weights. This schematic figure provides a clear overview of the analysis sequence, promoting transparency and reproducibility of the approach.

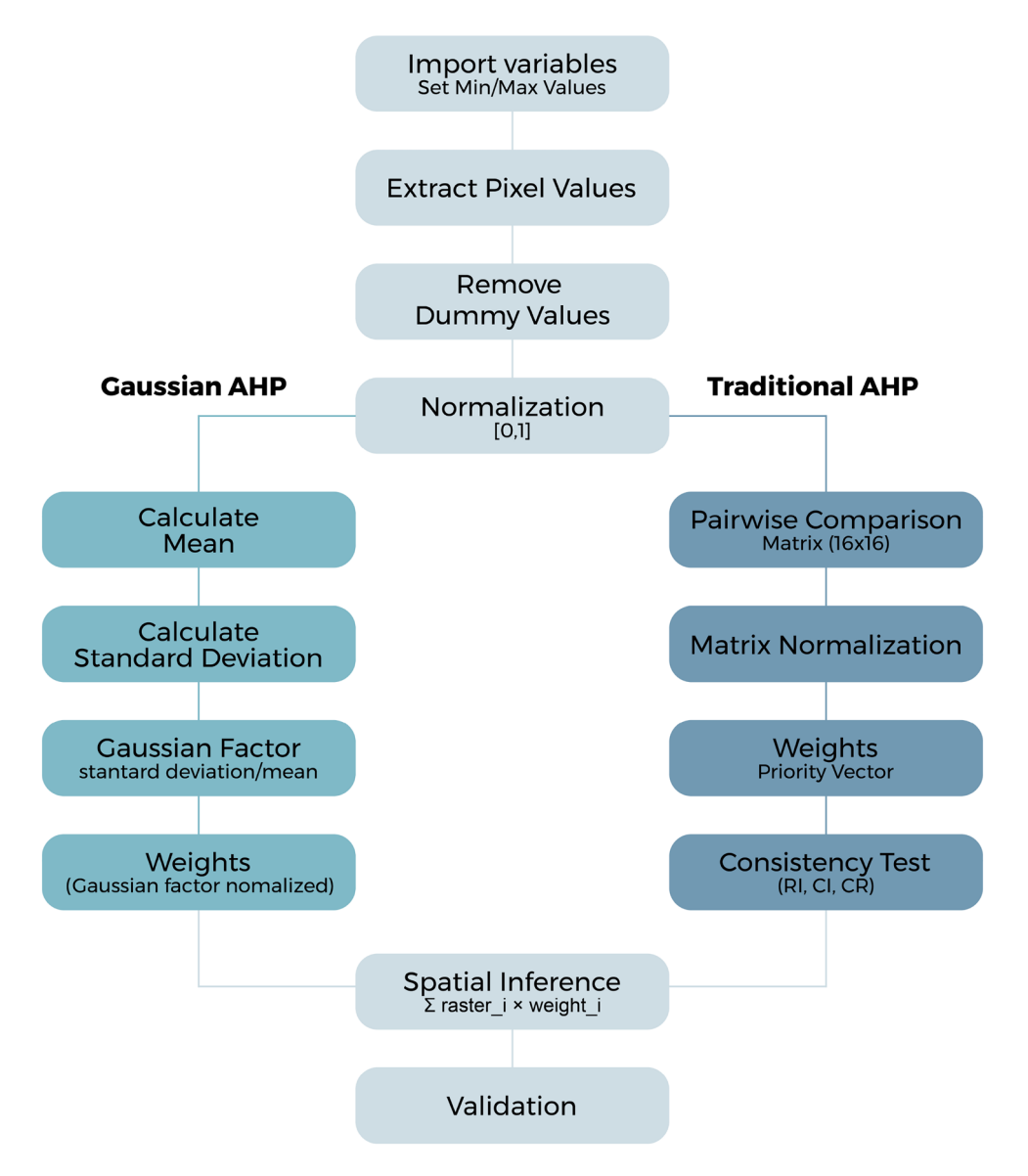


Fig. 3. Methodological flowchart.

Results Traditional AHP method

In the traditional AHP method, 120 pairwise comparisons were performed among 16 variables, resulting in a weighted decision matrix (Table 3). The variable slope emerged as the highest priority, with a relative weight of 18.2%, followed by relative slope position, TRI and geomorphology with 10.6%, and pedology with 8.60%, reflecting their considerable importance in the analyzed context. The consistency ratio obtained was 5.55%, indicating strong coherence in the preferences established during the comparison process. Priorities were determined using the principal eigenvector of the matrix, with a calculated eigenvalue of 17.332. Fig. 4 presents a graphical representation of the relative importance of all variables.

The susceptibility map was generated by multiplying each geospatial variable (raster) by its corresponding normalized weight. This process adjusts each variable's contribution based on its relevance, as determined in the previous calculation. Finally, the weighted results are summed pixel by pixel, resulting in a final layer that represents the integrated susceptibility, categorized into five classes: very low (14.19%), low (16.86%), moderate (28.76%), high (16.67%), and very high (23.52%). These results are consistent with findings from other studies^{74,97}, which have reported similar distributions of susceptibility classes in areas with comparable environmental and geological conditions. Fig. 5 presents the susceptibility map generated using the traditional AHP method. Among the five most relevant variables, areas classified with high or very high susceptibility are primarily located in regions with a slope between 23% and 46%, a relative slope position covering the entire range, and a TRI above 2.0. These areas are mainly found in terrains characterized as mountain ranges and escarpments, followed by high hills, low hills, and hills, where cambisol is the predominant soil type.

	V1	V2	V3	V4	V5	V6	V7	V8	V9	V10	V11	V12	V13	V14	V15	V16	NW
Slope (V1)	1	6	6	6	6	4	2	2	4	4	6	6	2	2	6	6	0.184
Aspect (V2)	1/6	1	1	1	1	1/2	1/4	1/4	1/2	1/2	1	4	1/4	1/4	1	1	0.032
Elevation (V3)	1/6	1	1	1	1	1/2	1/4	1/4	1/2	1/2	1	1	1/4	1/4	1	1	0.027
Plan curvature (V4)	1/6	1	1	1	1	1/2	1/4	1/4	1/2	1/2	1	1	1/4	4	1	1	0.041
Profile curvature (V5)	1/6	1	1	1	1	1/2	1/4	1/4	1/2	1/2	1	1	1/4	4	1	1	0.041
Convergence Index (V6)	1/4	2	2	2	2	1	1/2	1/2	1	1	2	2	1/2	1/2	2	2	0.053
Relative slope position (V7)	1/2	4	4	4	4	2	1	1	2	2	4	4	1	1	4	4	0.106
TRI (V8)	1/2	4	4	4	4	2	1	1	2	2	4	4	1	1	4	4	0.053
TWI (V9)	1/4	2	2	2	2	1	1/2	1/2	1	1	2	2	1/2	1/2	2	2	0.106
Distance to rivers (V10)	1/4	2	2	2	2	1	1/2	1/2	1	1	2	2	1/2	1/2	2	2	0.027
Land cover (V11)	1/6	1	1	1	1	1/2	1/4	1/4	1/2	1/2	1	1	1/4	1/4	1	1	0.053
Lithology (V12)	1/6	1/4	1	1	1	1/2	1/4	1/4	1/2	1/2	1	1	1/4	1/4	1	1	0.026
Geomorphology (V13)	1/2	4	4	4	4	2	1	1	2	2	4	4	1	1	4	4	0.106
Pedology (V14)	1/2	4	4	1/4	1/4	2	1	1	2	2	4	4	1	1	4	4	0.092
Rainfall (V15)	1/6	1	1	1	1	1/2	1/4	1/4	1/2	1/2	1	1	1/4	1/4	1	1	0.027
Distance to roads (V16)	1/6	1	1	1	1	1/2	1/4	1/4	1/2	1/2	1	1	1/4	1/4	1	1	0.027

Table 3. Normalized pairwise comparison matrix and normalized weights (NW). Vi corresponds to the i-th variable.

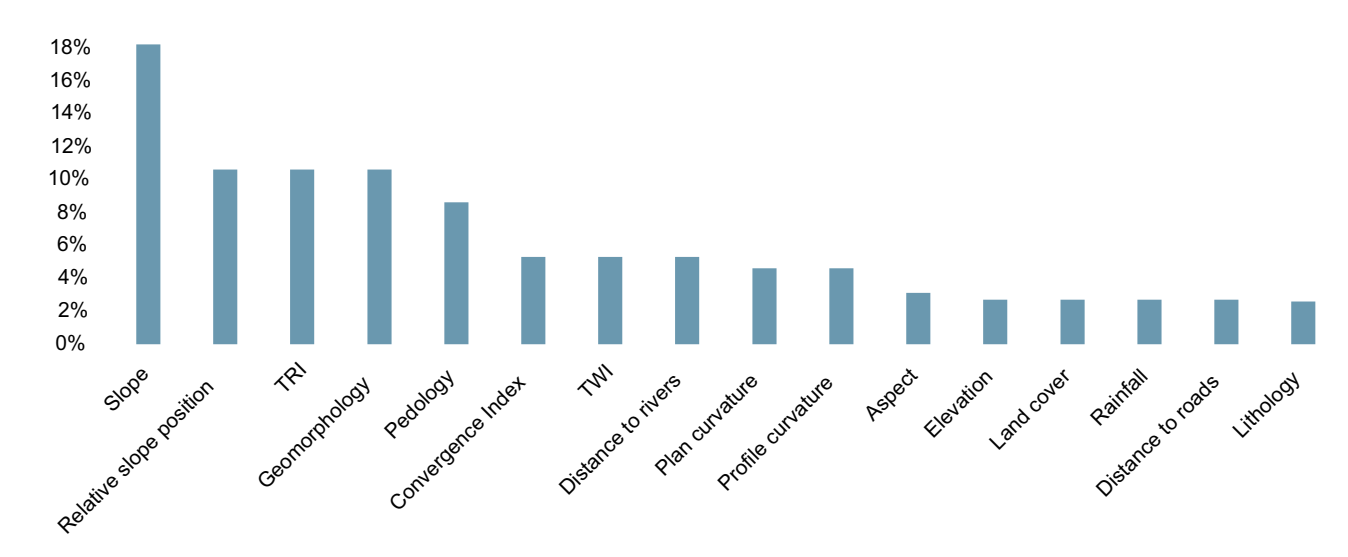


Fig. 4. Relative importance of variables according to the traditional AHP method.

Gaussian AHP method

According to the Gaussian AHP method, the most relevant variables for the event studied were geomorphology (18.22%), distance to rivers (15.65%), distance to roads (12.93%), elevation (9.26%), and land cover (8.32%). These values, derived from the normalized Gaussian factors, correspond to the normalized weights in the traditional AHP method. Fig. 6 illustrates the relevance assigned to each variable.

The susceptibility map generated using the Gaussian AHP method exhibited the following class distributions: very low (20.21%), low (15.55%), moderate (21.74%), high (16.19%), and very high (26.31%). Fig. 7 presents the resulting map. High and very high susceptibility areas are mainly located around 600 m away from roads and 160 m away from rivers, across all elevations, predominantly in mountain ranges and escarpments with cambisol soils, as well as in various hill terrains.

The susceptibility map was validated using two complementary approaches: the area under the ROC curve (AUC) and the analysis of landslide density across the susceptibility classes. For validation, a landslide inventory⁴¹ was used, which provided 97,742 samples divided into 70% for training and 30% for validation, as shown in close detail in Fig. 8. However, AUC, despite its widespread use in susceptibility studies, ignores the spatial distribution and density of events, potentially causing misleading results in areas with high spatial autocorrelation^{98,99}.

To address this limitation, the validation was strengthened by analyzing landslide density per susceptibility class, comparing observed event frequencies against random expectations. The use of a single-event inventory is

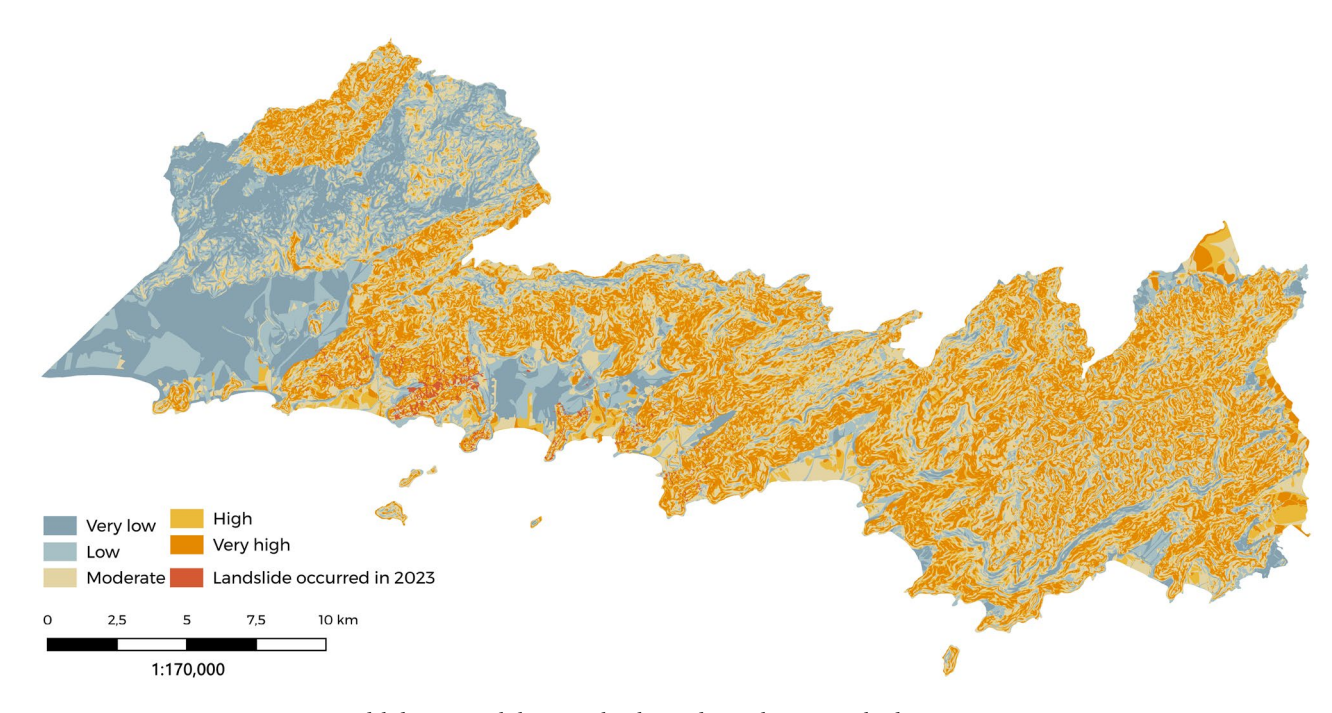


Fig. 5. Landslide susceptibility map by the traditional AHP method.

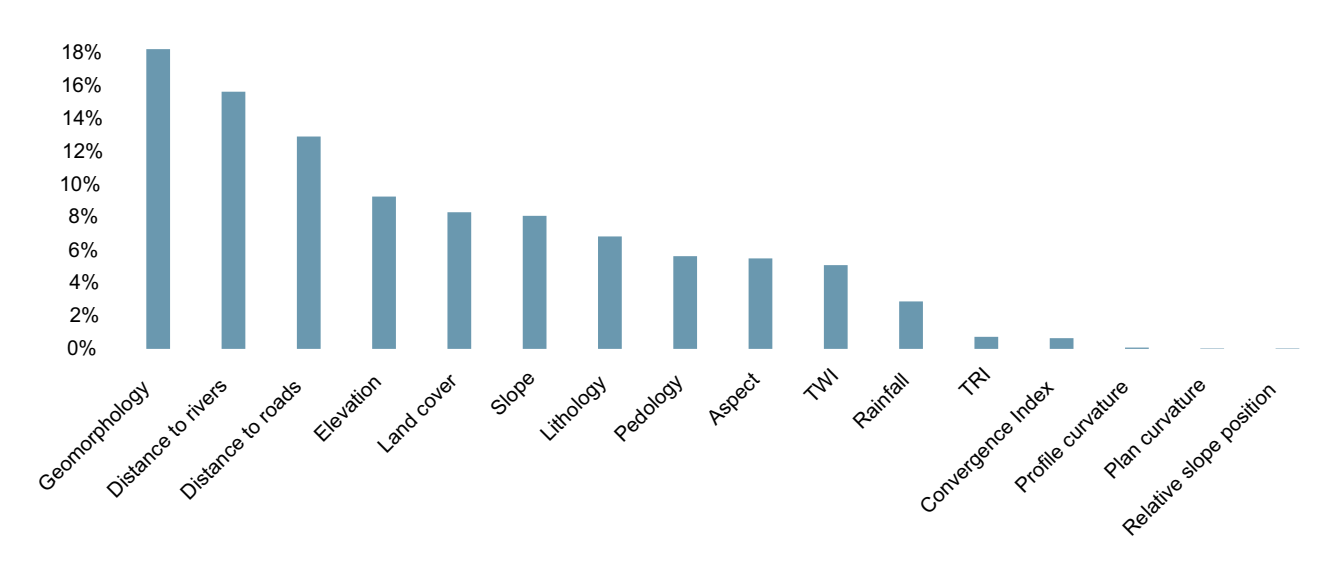


Fig. 6. Relative importance of variables according to the Gaussian AHP method.

justified by the exceptional magnitude, spatial extent, and quality of the 2023 São Sebastião disaster data, sourced from high-resolution aerial imagery and satellite scenes.

The comparative analysis between the traditional AHP and Gaussian AHP models indicates that the latter one demonstrated better overall performance across nearly all evaluated metrics. The ROC curve showed AUC values of 0.622 for traditional AHP and 0.636 for Gaussian AHP, indicating a slight edge of the improved model in distinguishing between areas with and without landslide occurrence. Although both values are below the 0.7 threshold — generally considered a sign of good discrimination — the Gaussian AHP also performed better in accuracy (0.6364 vs. 0.6229), and balanced accuracy (0.6356 vs. 0.6221). Sensitivity was also higher in the Gaussian model (0.3585 versus 0.3116), reflecting a greater ability to correctly identify negative areas. On the other hand, specificity and positive predictive value (PPV) were slightly higher in the traditional model (0.9325 vs. 0.9127, and 0.8212 vs. 0.8034, respectively), indicating its better accuracy in detecting positive areas (with landslides), as shown in Table 4. For all metrics, the p-values obtained through Mc Nemar's ¹⁰¹ test with a 95% confidence interval lay around 2×10^{-16} , indicating that there is significant difference between the accuracy parameters extracted for both models.

The relatively low sensitivity values observed may be due to the spatial distribution of validation samples, which are concentrated in one part of the study area. This spatial limitation might restrict the representation of

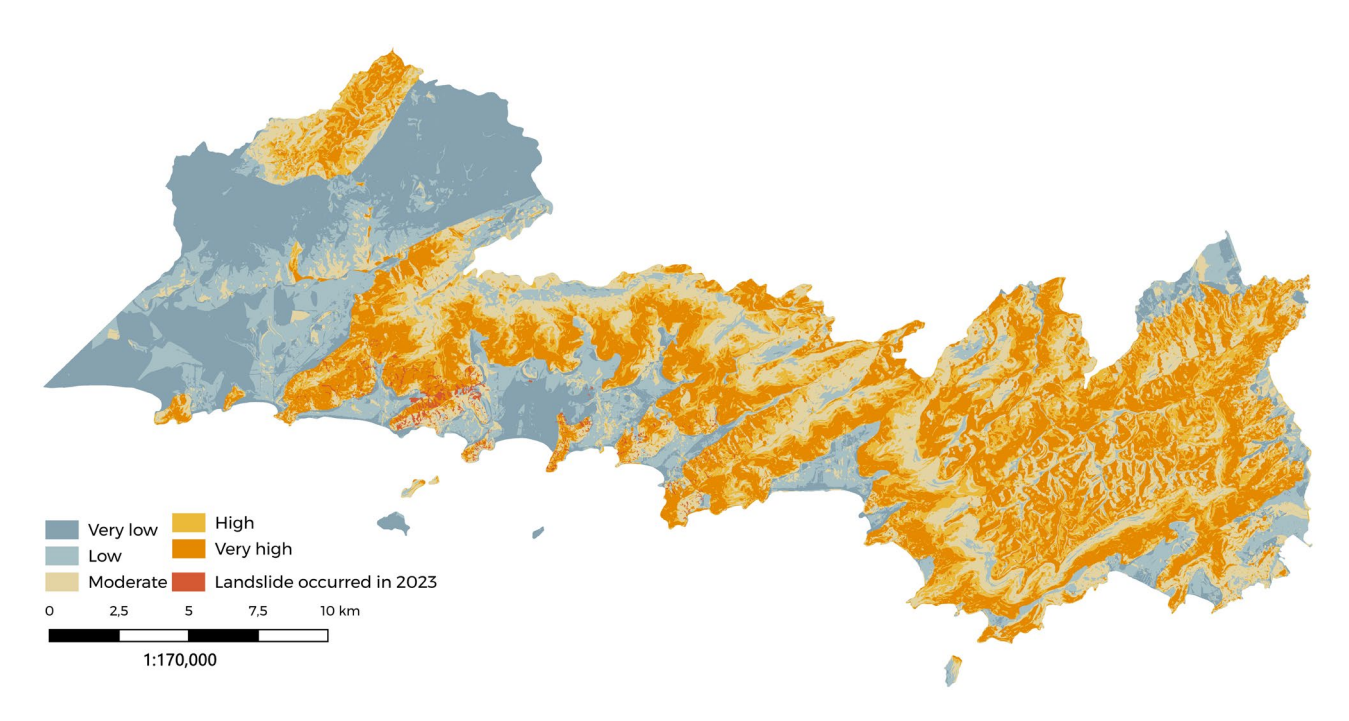


Fig. 7. Landslide susceptibility map by the Gaussian AHP method.



Fig. 8. Spatial distribution of landslide samples⁴¹ over a true color composite satellite image from June, 2025¹⁰⁰. (The data is sourced from a public Google Earth image available at https://earth.google.com/web/. The landslides data is sourced from a public repository available at https://zenodo.org/records/11120078. The processing software used is QGIS version 3.40.8, available at https://qgis.org/en/site/).

the region's environmental variability as a whole, affecting the model's ability to accurately generalize to other areas. Additionally, the strong spatial autocorrelation typical of landslide inventories, if not properly controlled, can inflate performance metrics in areas near the samples while underestimating prediction capacity in other regions. This highlights the need for validation methods that account for the spatial distribution of data, such as analyzing landslide density within each susceptibility class.

Table 5 compares the distribution of landslide susceptibility classes obtained by the traditional AHP and Gaussian AHP methods, highlighting key differences in how both approaches. While the traditional method shows a strong concentration of samples in the "Moderate" (29.52% training; 29.28% testing) and "Very high" (40.43% training; 40.44% testing) classes, the Gaussian AHP promotes a more balanced distribution, with a focus on increasing samples in lower risk classes, such as "Very low" (2.88% training and 2.91% testing, compared to 1.79% and 1.82% in the traditional method) and "Low" (5.92% training and 5.53% testing, compared to 4.75% and 4.51% in the traditional AHP). Additionally, the Gaussian approach slightly increases the representation of

Metric	Traditional AHP	Gaussian AHP
AUC	0.622	0.636
Accuracy	0.6229	0.6364
Balanced Accuracy	0.6221	0.6356
Sensitivity	0.3116	0.3585
Specificity	0.9325	0.9127
Positive Predictive Value (PPV)	0.8212	0.8034
Negative Predictive Value (NPV)	0.5766	0.5886

Table 4. Comparison of performance metrics between the traditional AHP and Gaussian AHP models.

		Traditional A	HP	Gaussian AHP			
Subregions Area (km ²)		Training (%)	Test (%)	Training (%)	Test (%)		
Very low	56.80	1.79	1.82	2.88	2.91		
Low	67.51	4.75	4.51	5.92	5.53		
Moderate	115.16	29.52	29.28	26.52	26.32		
High	66.71	23.52	23.94	19.07	19.06		
Very high	94.18	40.43	40.44	45.62	46.17		

Table 5. Key information of LS maps generated using traditional AHP and Gaussian AHP methods.

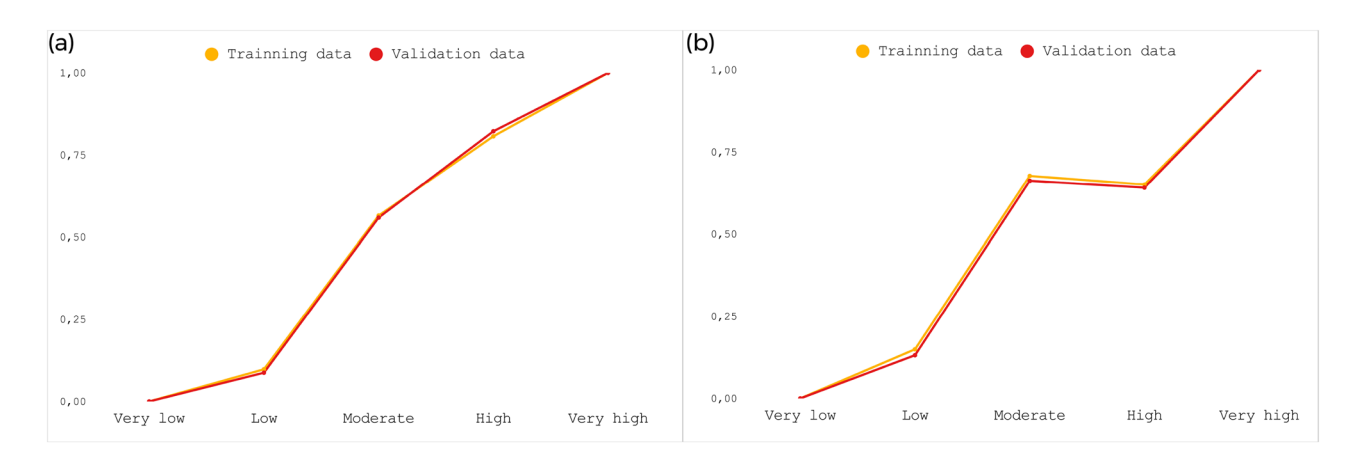


Fig. 9. Normalized landslide density distribution across susceptibility classes: **(a)** Traditional AHP, **(b)** Gaussian AHP.

the very high risk class (45.62% training and 46.17% testing), indicating a greater ability to identify critical areas. This behavior suggests that the Gaussian AHP approach can improve the spatial accuracy of the susceptibility classes, enhancing the performance of the model.

Figure 9 shows the analysis of normalized landslide density across the five susceptibility classes for both the traditional AHP and Gaussian AHP models, highlighting improvements in the Gaussian approach. The Gaussian AHP model displays a more balanced and distinctive distribution, with a curve showing smoother, more gradual transitions between low risk classes, unlike the sharper change seen in the traditional method. A key difference appears in the "moderate" class, where the Gaussian AHP demonstrates more stable and consistent behavior, whereas the traditional model shows a sharper increase followed by a slight decrease in the "high" class, creating an inflection point that indicates lower stability in distinguishing these intermediate categories. This suggests that the Gaussian AHP is more capable of capturing subtle variations in spatial risk, offering a more detailed and consistent classification of areas with intermediate susceptibility. Additionally, the Gaussian model yields slightly higher densities in the very low and low susceptibility classes, indicating better responsiveness in identifying transition zones and enhanced spatial representativeness. The smoother curve of the Gaussian AHP also suggests fewer artificial discontinuities in classification, leading to a more spatially coherent susceptibility map. The similarity between training and validation curves in both methods indicates no overfitting and good generalization ability, confirming the statistical robustness and operational reliability of the generated susceptibility maps. This underscores the improvements offered by the Gaussian AHP in risk management and land use planning.

In summary, both the traditional AHP and Gaussian AHP methods demonstrated consistent and coherent results, effectively highlighting areas with high and very high susceptibility to the studied event. While the traditional AHP method emphasized variables such as slope and relative slope position, the Gaussian AHP method prioritized geomorphology and proximity to rivers and roads, reflecting slight methodological differences in the weighting process. Despite these variations, the spatial distribution of susceptibility classes remained similar, with both methods identifying mountain ranges, escarpments, and cambisols as key contributing factors to high susceptibility. These findings underscore the robustness of the approaches and their potential applicability in similar environmental and geological contexts.

Discussion

The main difference noted between the results obtained from the two methods lies in the diverging importance assigned to the analyzed variables (Fig. 10). In the traditional AHP method, the first quartile of importance included the variables slope, relative slope position, TPI, and geomorphology. In contrast, in the Gaussian AHP method, these variables are not among the most relevant, except for geomorphology, which now holds the highest importance in the dataset. The variable slope, previously identified as the most relevant in the traditional AHP, was moved to the sixth position in the Gaussian AHP, while relative slope position also experienced a significant decrease, classified as the least relevant. This shift indicates that the Gaussian AHP's focus on statistical variability prioritizes factors with greater spatial heterogeneity, while the traditional AHP's dependence on expert-based pairwise judgments emphasizes geomorphic characteristics and slope gradient more heavily.

In addition to geomorphology, other variables gained prominence in the Gaussian AHP method, including distance to rivers, distance to roads, elevation, aspect, and land cover. Conversely, the variable pedology presented a slight reduction in its relative importance. Meanwhile, the variables TWI and rainfall maintained similar relevance across both methods, indicating a degree of consistency in their impact assessment. Notably, the prominence of proximity factors (rivers and roads) in the Gaussian AHP results matches the spatial clustering of landslide events near infrastructure and drainage lines, supporting the method's ability to identify real-world triggers that may be underrepresented in subjective weightings.

The observed differences in the assignment of importance between the traditional AHP and Gaussian AHP methods can likely be attributed to the distinct ways these approaches handle variability and weighting. The traditional AHP relies on pairwise comparisons to derive weights, which are directly influenced by subjective judgments and the consistency of the decision-maker preferences. In contrast, the Gaussian AHP method incorporates statistical measures, such as the standard deviation and mean, to calculate normalized Gaussian factors, emphasizing the variability within the dataset. This statistical approach can lead to higher weights for variables with greater spatial heterogeneity, as seen with the distance to rivers and distance to roads, which gained prominence in the Gaussian AHP method. Additionally, the smoothing effect of Gaussian normalization might diminish the relative influence of variables that are more uniformly distributed across the study area, such as slope and relative slope position, which held higher importance in the traditional AHP. These methodological differences highlight the sensitivity of weighting processes to both subjective inputs and data-driven factors, ultimately shaping the prioritization of variables in distinct ways. Moreover, by reducing subjective bias, the Gaussian AHP method seems to improve the match between model-based weights and the actual spatial patterns of landslides, as shown by better AUC and balanced accuracy scores. This indicates that in areas with diverse terrain and complex land use interactions, data-driven weighting can produce more reliable susceptibility predictions.

Compared to the traditional AHP method, the very low class increased by 6.02%, while the low class decreased by 1.32% in the Gaussian AHP. The moderate and high classes experienced decreases of 7.02% and 0.47%, respectively, whereas the very high class increased by 2.79%. These differences reflect adjustments in the

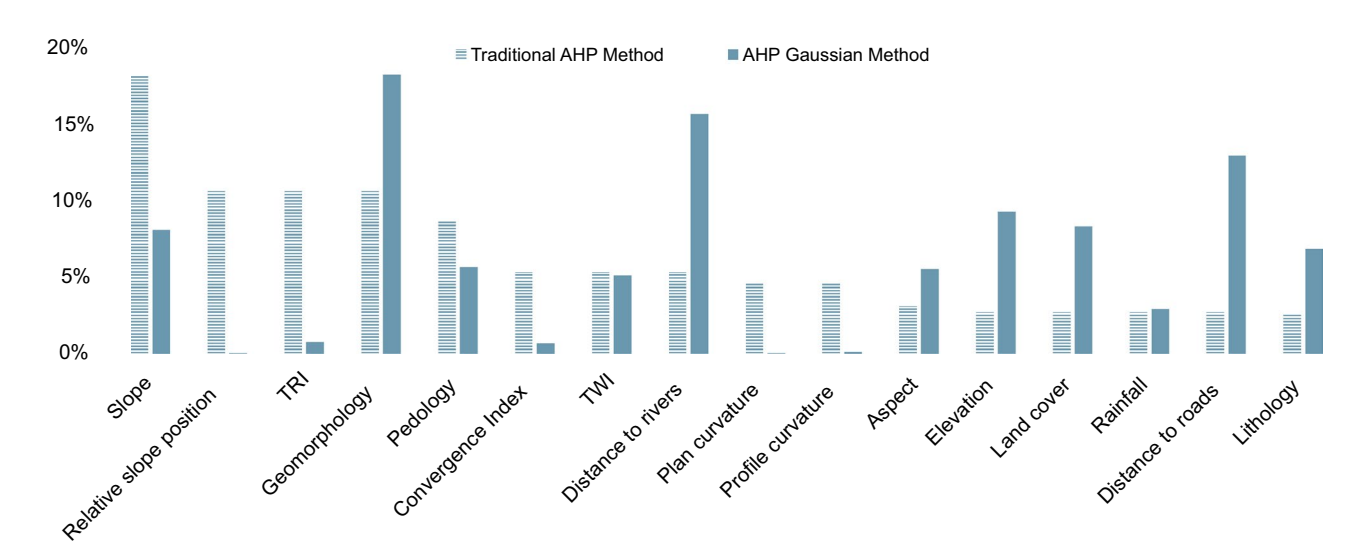


Fig. 10. Relative importance of variables according to the methods.

weights assigned to the variables by the Gaussian AHP method, which incorporates normalized Gaussian factors in its weighting process. Despite these variations, both methods produce susceptibility maps with consistent overall distributions. The highest susceptibility classes (high and very high) remain relatively close in percentage terms, ensuring effective identification of the most vulnerable areas. Notably, the improvements in the very high class under Gaussian AHP align with its higher sensitivity, showing a clearer separation of critical zones without losing overall map coherence.

Furthermore, the overall uncertainty analysis (Fig. 11) between the two methods revealed a value of 56.16%, with class-specific results distributed as follows: very low (53.20%), low (76.47%), moderate (76.42%), high (85.15%), and very high (65.34%). These metrics illustrate how the differences between the methods are reflected across classes, highlighting the unique characteristics of each approach in weight assignment and final classification. Nevertheless, the results confirm that both methods are capable of efficiently identifying areas of higher susceptibility, providing reliable support for decision-making in risk management contexts. The slightly lower uncertainty in the very high classes under Gaussian AHP indicates increased model confidence where it turns out to be crucially important for hazard mitigation.

When examining the outcomes of the susceptibility analysis limited to areas affected by landslides in 2023 (Fig. 12), it was observed that in both models, the high and very high classes predominated, together accounting for nearly 70% of the analyzed area. In the traditional AHP method, the classes distributions were: very high (38.46%), high (28.78%), moderate (22.07%), low (7.39%), and very low (3.29%). With the Gaussian AHP method, the distributions were: very high (42.19%), high (26.46%), moderate (18.20%), low (7.30%), and very low (5.85%). A comparison of the results reveals that in the Gaussian AHP method, the very high class increased by 3.73%, followed by a 2.56% rise in the very low class. Conversely, the low, moderate, and high classes experienced decreases of 0.09%, 3.87%, and 2.32%, respectively. These variations highlight the distinct characteristics of the two methods in weighting and classification, while both consistently identify areas with higher susceptibility. The focus of this analysis highlights the practical importance of the Gaussian AHP method for post-event evaluations, precisely when capturing both extremes of vulnerability can help direct quick resource deployment for emergency response and infrastructure inspection.

The estimated 24-hour accumulated precipitation for the analyzed event ranged from 106.43 to 683 mm (Fig. 13), based on data from the São Paulo Weather Radar¹⁰² and the São Sebastião Civil Defense (pluviometric station). The highest rainfall concentration occurred in the western-central portion of the study area, which also registered the greatest number of landslides, indicating a strong correlation between extreme precipitation and slope instability. While some areas are inherently more susceptible due to geological and geomorphological factors, these findings reinforce the role of rainfall as the primary trigger for such events⁴⁷. This highlights the importance of continuous precipitation monitoring in landslide-prone regions and the integration of meteorological data into risk assessment and early warning systems.

Despite significant precipitation levels exceeding 300 mm in some areas of the study's western region, specific locations did not experience any landslides. This absence of mass movements could be attributed to several factors, including (i) a more advanced stormwater drainage system that effectively channels excess water and reduces soil saturation, (ii) engineered structures designed to reinforce slopes and mitigate the impacts of intense rainfall, and (iii) specific geomorphological characteristics, such as variations in soil-bearing capacity, lithology, vegetation cover, and terrain development, all of which influence the overall stability of the landscape. Additionally, differences in land use and human interventions, such as deforestation, construction practices, and slope modifications, may also play a role in preventing or intensify landslides under extreme rainfall conditions. It is important to mention that these factors were not included as input variables in the modeling approach, which primarily focuses on susceptibility assessments based on geospatial and environmental parameters. As a result, while the model effectively identifies high-risk areas, it may not fully capture localized resilience mechanisms that contribute to variations in landslide occurrence across the study area.

While the traditional AHP provides a familiar, expert-driven framework, the Gaussian AHP method delivers a more data-centric weighting scheme that better reflects observed landslide patterns and yields improvements in

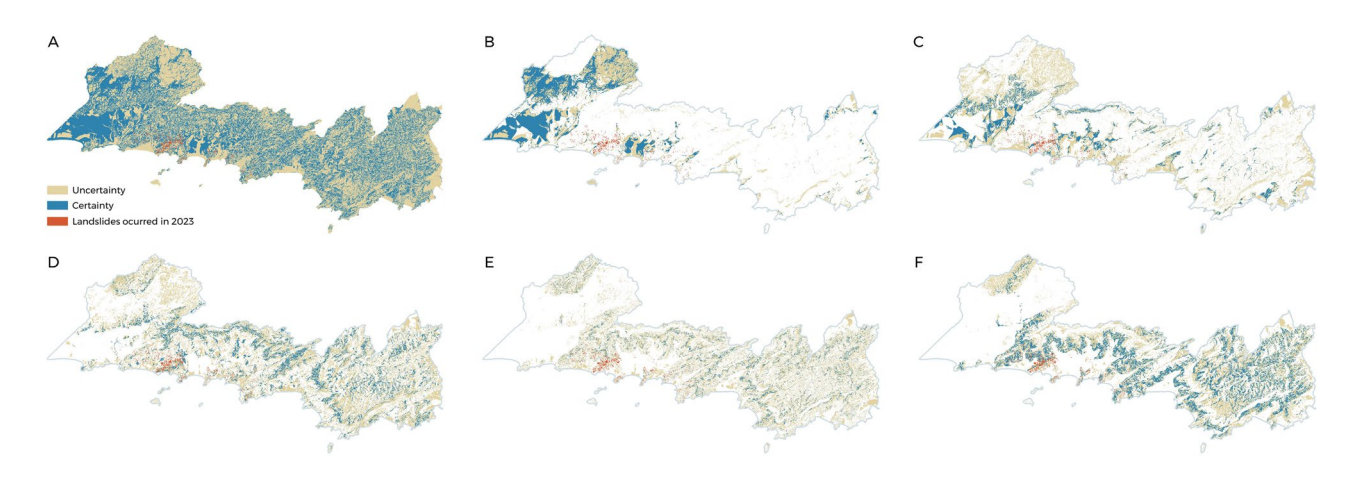


Fig. 11. Uncertainty analysis: (A) Overall, (B) Very low, (C) Low, (D) Moderate, (E) High, and (F) Very high.

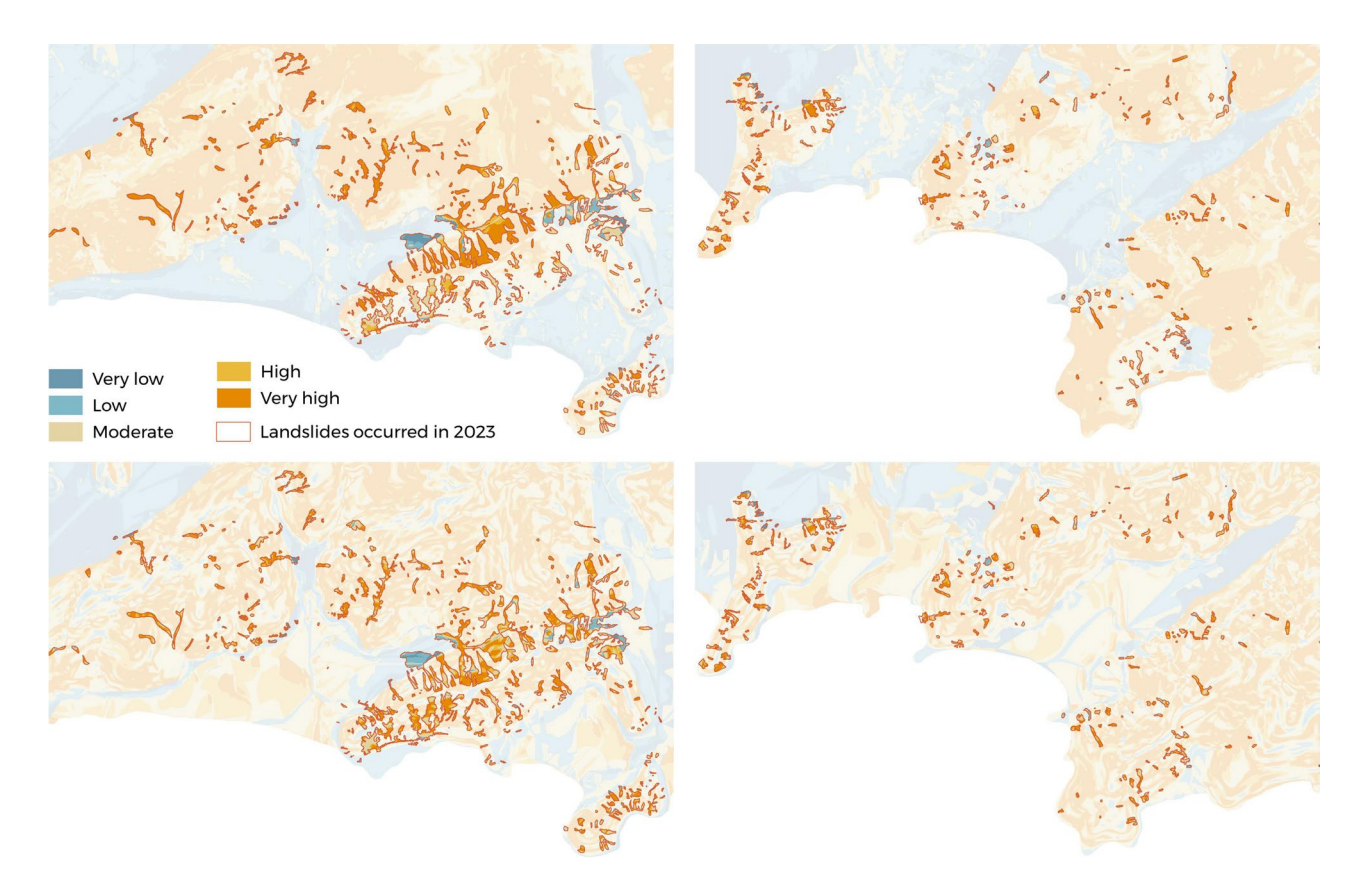


Fig. 12. Details of the susceptibility analysis related to the 2023 event, superimposed on the landslides assessed by 41 and integrally shown in Figure 1d: Gaussian AHP results (above) and traditional AHP results (below).

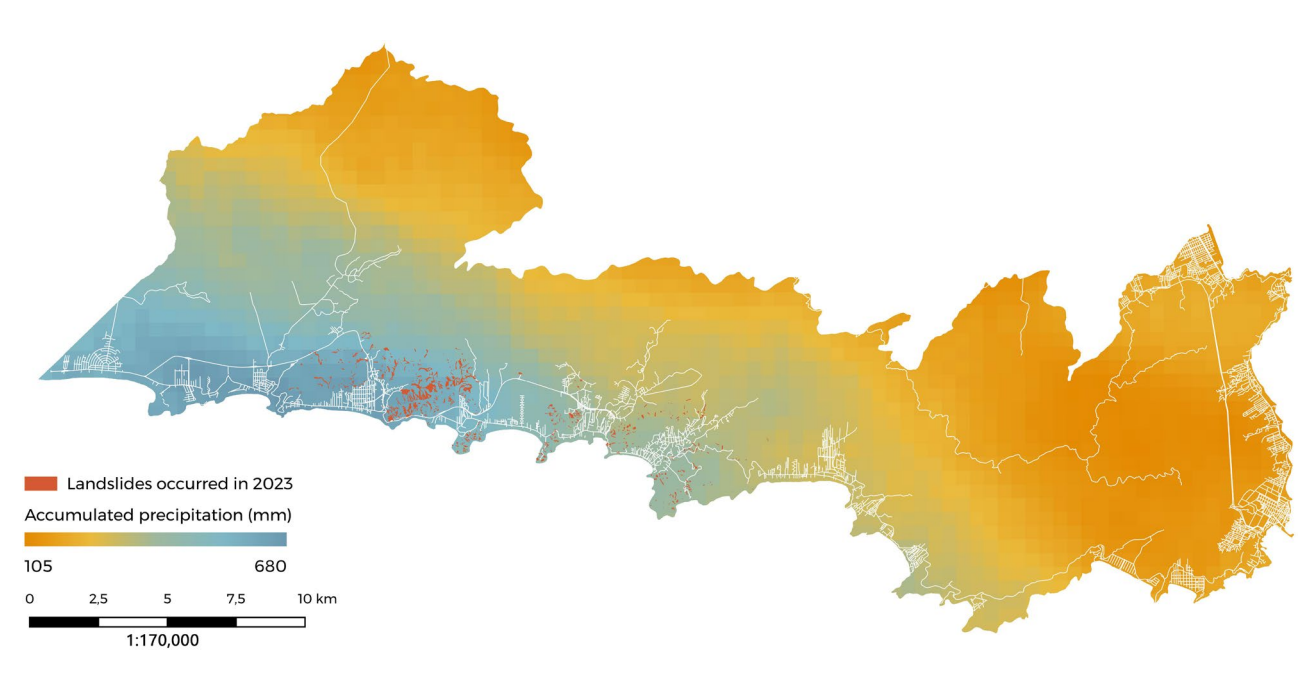


Fig. 13. The estimated 24-hour accumulated precipitation in São Sebastião on 19 February 2023.

predictive performance. These findings suggest that integrating statistical variability into multi-criteria decision processes can enhance the objectivity and operational usefulness of susceptibility models in heterogeneous landscapes.

The Gaussian AHP model offers significant contributions by replacing the subjective paired comparisons of traditional AHP with a statistical approach using metrics such as mean and standard deviation to determine factor weights. This method reduces the subjectivity in expert judgments, emphasizes the spatial variability of data, and assigns greater importance to variables with greater heterogeneity, such as proximity to rivers and roads. This feature is especially useful in geologically complex contexts, where the spatial distribution of influencing factors can differ greatly. Moreover, the Gaussian AHP allows for scalable multi-criteria analysis, enabling the integration of large amounts of geospatial data without losing the model's internal consistency and not demanding proportionally intensive computing infrastructure either in face of its low cost. These features make it a helpful tool for landslide susceptibility analysis in large, environmentally complex areas from an operational perspective.

However, the Gaussian AHP model has certain limitations that should be considered. One of them is its sensitivity to data distribution: variables with a uniform distribution, such as slope, may have their importance underestimated, while the presence of outliers or biases in data collection can distort the assigned weights. Additionally, its reliance on high-resolution quantitative data may restrict its applicability in cases with limited computational infrastructure or scarce data availability. Another limitation is the lack of dynamic validation, such as including human-related factors or drainage efficiency, which may affect the model's ability to account for local resilience mechanisms, including engineering interventions that mitigate risks or efficient drainage systems. These gaps can lead to either an underestimation or overestimation of susceptibility in specific areas.

As mentioned earlier, the AHP method has been widely used for landslide susceptibility assessment ^{22–35,47,97,103}; however, to our knowledge, no research in the indexed literature has explored the application of Gaussian AHP for this purpose. Nonetheless, some studies have incorporated Gaussian processes into their methodology. Colkesen et al. ¹⁰⁴ explored the use of kernel-based Gaussian process regression and support vector regression (SVM) to create a landslide susceptibility map in a district of Trabzon, Turkey. Xie et al. ¹⁰⁵ proposed a landslide hazard assessment using an SVM as the main model and a Bayesian Optimization (BO) algorithm for parameter tuning; this parameter optimization technique was based on Gaussian process regression. On their turn, Gao et al. ¹⁰⁶ applied Gaussian process classification (GPC) and an improved weight-based generalized objective function to evaluate hazard, vulnerability, and risk of high-mountain landslides in Southwest China.

Despite differences in variable ranking between the traditional AHP and the Gaussian AHP, both methods have demonstrated consistency in identifying critical landslide susceptibility zones. To further enhance the model, integrating Gaussian AHP with machine learning techniques is recommended, as this would improve the ability to detect nonlinear relationships and complex data patterns, thereby increasing predictive accuracy. Additionally, incorporating real-time climate data, such as precipitation and soil moisture, could address gaps in modeling immediate triggers like extreme rainfall, which is often linked to landslide events. This integration would foster a more comprehensive and dynamic approach, increasing the model's reliability in the face of climate change and rapid urbanization.

Finally, it is worth highlighting that other authors conducted landslides susceptibility analyses for the same study area of this research, but using either statistical or machine learning models. The work conducted by Coelho et al. (2025)¹⁰⁷ ought to be mentioned, in which different environmental variables (slope, aspect, curvatures, digital elevation models - DEMs of varying spatial resolutions, and the Topographic Position Index - TPI) were combined through logistic regression. The authors used the same reference data of our study and attained accuracy values ranging from 0.6630 to 0.7067, and AUC values from 0.7101 to 0.7840, respectively for the 5-meter and 30-meter DEMs. Another work¹⁰⁸ carried out for São Sebastião drove environmental (elevation, slope, aspect, geology, pedology, land use and land cover, normalized difference vegetation index - NDVI) and climatic (72-hour accumulated precipitation) variables in a multilayer perceptron neural network. The author obtained 1.00 for Precision, 0.86 for Recall, and 0.92 for F1-Score.

Alcântara et al. (2024)⁴⁶ compared manifold machine learning models, namely random forest (RF), gradient boosting (GB), support vector machine (SVM), artificial neural network (ANN), and k-nearest neighbors (k-NN), which were driven by input data like slope, soil saturation, relief dissection, geomorphology, geology, Topographic Position Index (TPI), Soil Moisture Index (SMI), land use and land cover (LULC) information extracted from Planet imagery, and the 72-hour accumulated precipitation. RF and GB reached the highest accuracy (0.996) and F1-Score (0.665) values, followed by ANN (accuracy of 0.993 and F1-Score of 0.663), k-NN (accuracy of 0.986 and F1-Score of 0.660) and SVM (accuracy of 0.597 and F1-Score of 0.344). The AUC in this study presented a diverging behavior in relation to these two previous accuracy metrics since GB was ranked first (AUC of 0.963), succeeded by ANN (AUC of 0.961), SVM (AUC of 0.930), RF (AUC of 0.911), and k-NN (AUC of 0.826).

We ought though to emphasize that addressing direct comparisons between our results and the results formerly presented specifically for São Sebastião is purposeless, since these works employed diverse sets of input variables, in some cases also different reference data, and/or used partially distinct accuracy metrics. The competitive advantage of the Gaussian AHP approach, explored in this work, lies on its operational straightforwardness. In other words, the Gaussian AHP method trades simplicity for performance. Refined statistical and machine learning models usually achieve better results. Nevertheless, they are complex and require a level of expertise commonly unavailable among the local government practitioners.

Conclusion

The comparative evaluation confirmed that both the traditional AHP and the Gaussian AHP approaches reliably delineate zones of high and very high landslide susceptibility, demonstrating their suitability for risk assessment. However, the Gaussian AHP method consistently outperformed the traditional AHP, achieving higher AUC (0.636 vs. 0.622), accuracy (0.6364 vs. 0.6229), balanced accuracy (0.6356 vs. 0.6221), as well as greater sensitivity (0.3585 vs. 0.3116), thereby showing superior discriminative power and reliability. While traditional

AHP placed greatest emphasis on slope and relative slope position, Gaussian AHP shifted weight values toward geomorphology and proximity to rivers and roads—variables exhibiting greater spatial heterogeneity—which more closely align with observed landslide clusters in São Sebastião.

Despite methodological differences, the overall spatial distribution of susceptibility classes remained coherent between models, with mountainous escarpments persistently identified as the most vulnerable areas. The uncertainty analysis showed that Gaussian AHP reduced classification ambiguity in the highest risk category (65.34% of ambiguity), indicating improved confidence where it is most critical for hazard mitigation. Rainfall emerged again as the predominant trigger, with 24-hour accumulations exceeding 300 mm in the western-central sector correlating strongly with landslide occurrence—even though engineered drainage and slope reinforcements likely mitigated failures in some high-rainfall areas. This finding reinforces the necessity of integrating real-time meteorological monitoring into future susceptibility frameworks. Overall, the data-driven Gaussian enhancement reduces subjective bias and aligns model outputs more closely with empirical patterns, leading to improvements in predictive performance. As directions for future work, we recommend combining the Gaussian AHP weighting scheme with machine learning classifiers (e.g., random forests or gradient boosting) to capture nonlinear interactions among conditioning factors, and incorporating dynamic variables such as soil moisture and land use change to further refine temporal responsiveness and predictive accuracy.

Data availability

Data is provided within the manuscript or supplementary information files.

Received: 19 April 2025; Accepted: 25 September 2025

Published online: 31 October 2025

References

- Ozturk, U. et al. How climate change and unplanned urban sprawl bring more landslides. Nature 608, 262–265. https://doi.org/1 0.1038/d41586-022-02141-9 (2022).
- Intergovernmental Panel on Climate Change. Climate Change 2001: Impacts, Adaptation, and Vulnerability: Contribution of Working Group II to the Third Assessment Report of the Intergovernmental Panel on Climate Change (Cambridge University Press, 2001)
- 3. Petley, D. The 26 to 28 september 2024 landslide disaster in Nepal (2024).
- 4. Survey, U. G. Usgs landslide event team activated in wake of hurricane helene (2018).
- Nava, L. et al. Brief Communication: AI-driven rapid landslides mapping following the 2024 Hualien City Earthquake in Taiwan. Natural Hazards and Earth System Sciences Discussions 2024, 1–9. https://doi.org/10.5194/nhess-2024-146 (2024).
- Froude, M. J. & Petley, D. N. Global fatal landslide occurrence from 2004 to 2016. Natural Hazards and Earth System Sciences 18, 2161–2181. https://doi.org/10.5194/nhess-18-2161-2018 (2018).
- Brazilian Institute of Geography and Statistics. Suscetibilidade a deslizamentos do Brasil: primeira aproximação (IBGE, Rio de Janeiro, 2019). https://biblioteca.ibge.gov.br/index.php/biblioteca-catalogo?view=detalhes&id=2101684.
- 8. Highland, L. M. & Bobrowsky, P. The landslide handbook a guide to understanding landslides https://doi.org/10.3133/cir1325 (2008).
- Quevedo, R. P. et al. Land use and land cover as a conditioning factor in landslide susceptibility: a literature review. Landslides 20, 967–982. https://doi.org/10.1007/s10346-022-02020-4 (2023).
- 10. Alcántara-Ayala, I. Landslides in a changing world. Landslides https://doi.org/10.1007/s10346-024-02451-1 (2025).
- Guzzetti, F., Carrara, A., Cardinali, M. & Reichenbach, P. Landslide hazard evaluation: a review of current techniques and their application in a multi-scale study, central italy. Geomorphology 31, 181–216. https://doi.org/10.1016/S0169-555X(99)00078-1 (1999)
- 12. Guo, Z., Tian, B., Zhu, Y., He, J. & Zhang, T. How do the landslide and non-landslide sampling strategies impact landslide susceptibility assessment? a catchment-scale case study from china. *Journal of Rock Mechanics and Geotechnical Engineering* 16, 877–894. https://doi.org/10.1016/j.jrmge.2023.07.026 (2024).
- 13. Guo, Z. et al. Pslsa v2.0: An automatic python package integrating machine learning models for regional landslide susceptibility assessment. *Environmental Modelling & Software* 186, 106367. https://doi.org/10.1016/j.envsoft.2025.106367 (2025).
- Shano, L., Raghuvanshi, T. K. & Meten, M. Landslide susceptibility evaluation and hazard zonation techniques a review. Geoenvironmental Disasters 7, 18. https://doi.org/10.1186/s40677-020-00152-0 (2020).
- 15. Singh, K., Bhardwaj, V., Sharma, A. & Thakur, S. A comprehensive review on landslide susceptibility zonation techniques. *Quaestiones Geographicae* 43, 79–91. https://doi.org/10.14746/quageo-2024-0005 (2024).
- Pardeshi, S. D., Autade, S. E. & Pardeshi, S. S. Landslide hazard assessment: recent trends and techniques. SpringerPlus 2, 523. https://doi.org/10.1186/2193-1801-2-523 (2013).
- 17. Dias, H. C., Hölbling, D. & Grohmann, C. H. Landslide susceptibility mapping in brazil: A review. *Geosciences* 11, https://doi.org/10.3390/geosciences11100425(2021).
- 18. Sujatha, E. R. & Sudharsan, J. S. Landslide susceptibility mapping methods—a review. In *Landslide: Susceptibility, Risk Assessment and Sustainability: Application of Geostatistical and Geospatial Modeling*, 87–102, https://doi.org/10.1007/978-3-031-56591-5_4(Springer Nature Switzerland, Cham, 2024).
- Saaty, T. L. A scaling method for priorities in hierarchical structures. *Journal of Mathematical Psychology* 15, 234–281. https://doi.org/10.1016/0022-2496(77)90033-5 (1977).
- Emrouznejad, A. & Marra, M. The state of the art development of ahp (1979–2017): a literature review with a social network analysis. *International Journal of Production Research* 55, 6653–6675. https://doi.org/10.1080/00207543.2017.1334976 (2017).
- Dean, J. A Golden Decade of Deep Learning: Computing Systems & Applications. Daedalus 151, 58–74. https://doi.org/10.1162/daed/a01900 (2022).
- 22. Madzík, P. & Falát, L. State-of-the-art on analytic hierarchy process in the last 40 years: Literature review based on latent dirichlet allocation topic modelling. *PLoS One* 17, e0268777. https://doi.org/10.1371/journal.pone.0268777 (2022).
- 23. El Jazouli, A., Barakat, A. & Khellouk, R. Gis-multicriteria evaluation using AHP for landslide susceptibility mapping in Oum Er Rbia high basin (Morocco). *Geoenvironmental Disasters* 6, 3. https://doi.org/10.1186/s40677-019-0119-7 (2019).
- 24. Huang, F. et al. Comparisons of heuristic, general statistical and machine learning models for landslide susceptibility prediction and mapping. *CATENA* **191**, 104580. https://doi.org/10.1016/j.catena.2020.104580 (2020).
- Sonker, I., Tripathi, J. N. & Singh, A. K. Landslide susceptibility zonation using geospatial technique and analytical hierarchy process in sikkim himalaya. Quaternary Science Advances 4, 100039. https://doi.org/10.1016/j.qsa.2021.100039 (2021).
- Panchal, S. & Shrivastava, A. K. Landslide hazard assessment using analytic hierarchy process (ahp): A case study of national highway 5 in india. Ain Shams Engineering Journal 13, 101626. https://doi.org/10.1016/j.asej.2021.10.021 (2022).

- 27. Zhou, J. et al. Landslide susceptibility assessment using the analytic hierarchy process (ahp): A case study of a construction site for photovoltaic power generation in yunxian county, southwest china. Sustainability 15 (2023).
- 28. Kucuker, D. M. Analyzing landslide susceptibility of forest roads by analytical hierarchy process (ahp) in the of forest planning unit of turkiye. *Natural Hazards* https://doi.org/10.1007/s11069-024-06882-w (2024).
- 29. Liu, X., Shao, S. & Shao, S. Landslide susceptibility zonation using the analytical hierarchy process (ahp) in the great xi'an region, china. *Scientific Reports* 14, https://doi.org/10.1038/s41598-024-53630-y(2024).
- 30. Ou, L., Huang, C. & Cao, Y. Research on landslide hazard assessment based on improved analytic hierarchy process optimizing multiple rainfall indicators. *Discover Applied Sciences* 6, 409. https://doi.org/10.1007/s42452-024-06119-2 (2024).
- 31. Gulbet, E. & Getahun, B. Landslide susceptibility mapping using frequency ratio and analytical hierarchy process method in awabel woreda, ethiopia. *Quaternary Science Advances* 16, 100246. https://doi.org/10.1016/j.qsa.2024.100246 (2024).
- 32. Mengstie, L., Nebere, A., Jothimani, M. & Taye, B. Landslide susceptibility assessment in addi arkay, ethiopia using gis, remote sensing, and ahp. *Quaternary Science Advances* 15, 100217. https://doi.org/10.1016/j.qsa.2024.100217 (2024).
- 33. Singh, M., Khajuria, V., Singh, S. & Singh, K. Landslide susceptibility evaluation in the beas river basin of north-western himalaya: A geospatial analysis employing the analytical hierarchy process (ahp) method. *Quaternary Science Advances* 14, 100180. https://doi.org/10.1016/j.qsa.2024.100180 (2024).
- 34. Lahcen Dahmani, H. N., Said Laaribya & Dindaroglu, T. Landslide hazard mapping in chefchaouen, morocco: Ahp-gis integration. *International Journal of Environmental Studies* **0**, 1–18, doi:10.1080/00207233.2024.2412483 (2024).
- 35. Arvindd Kshetrimayum, R. H. & Goyal, A. Exploring different approaches for landslide susceptibility zonation mapping in manipur: a comparative study of ahp, fr, machine learning, and deep learning models. *Journal of Spatial Science* **0**, 1–30, https://doi.org/10.1080/14498596.2024.2368156(2024).
- 36. Hontoria, E. & Munier, N. Uses and Limitations of the AHP Method A Non-Mathematical and Rational Analysis (2021).
- 37. Santos, M. d., Costa, I. P. d. A. & Gomes, C. F. S. Multicriteria decision-making in the selection of warships: A new approach to the ahp method. *International Journal of the Analytic Hierarchy Process* 13, https://doi.org/10.13033/ijahp.v13i1.833(2021).
- 38. Russo, A. C. & Russo, E. Application of the ahp-gaussian method to support the prioritization of workers' health actions in brazil, based on data from datasus. *Gestão &Produção* 31, 10. https://doi.org/10.1590/1806-9649-2024v31e10423 (2024).
- 39. Instituto Brasileiro de Geografia e Estatística (IBGE). Downloads geociências. https://www.ibge.gov.br/geociencias/download s-geociencias.html (2025). Acesso em: 19 jul. 2025.
- 40. European Union Copernicus Sentinel data. Sentinel satellite image provided by copernicus open access hub. https://apps.sentinelhub.com/eo-browser/ (2025). Contains modified Copernicus Sentinel data [2025], processed by the author. Accessed July 19, 2025
- 41. Coelho, R. D., Viana, C. D., Dias, V. C. & Grohmann, C. H. Landslides of the 2023 summer event of são sebastião, southeastern brazil: spatial dataset. *Brazilian Journal of Geology* https://doi.org/10.1590/2317-4889202420240006 (2024).
- Camarinha, P. I. M. Analysis of Vulnerability to Natural Disasters Caused by Landslides Considering the Context of Climate Change, in Serra do Mar in São Paulo State. Phd thesis in earth system science, National Institute for Space Research, São José dos Campos, SP, Brazil (2016). http://mtc-m21b.sid.inpe.br/ibi/8JMKD3MGP3W34P/3LT6C4S.
- 43. Marengo, J. A. et al. Heavy rains and hydrogeological disasters on february 18th-19th, 2023, in the city of são sebastião, são paulo, brazil: from meteorological causes to early warnings. *Natural Hazards* 120, 7997–8024. https://doi.org/10.1007/s11069-024-0655 8-5 (2024).
- 44. Veloso, V. Q. et al. Application of the debris-flow hazard index for pipelines in the context of the hydrogeological disaster of february 2023 in são sebastião, serra do mar, brazil. *Landslides* https://doi.org/10.1007/s10346-024-02319-4 (2024).
- Moço, G. A. et al. Unsupervised change detection methods applied to landslide mapping: Case study in são sebastião, brazil. *Transactions in GIS* 28, 2557–2845. https://doi.org/10.1111/tgis.13256 (2024).
- Alcântara, E., Baião, C. F., Guimarães, Y. C., Mantovani, J. R. & Marengo, J. A. Machine learning approaches for mapping and predicting landslide-prone areas in são sebastião (southeast brazil). *Natural Hazards Research* https://doi.org/10.1016/j.nhres.20 24.10.003 (2024).
- 47. Alcântara, E., Baião, C. F., Guimarães, Y. C., Marengo, J. A. & Mantovani, J. R. Climate change-induced shifts in landslide susceptibility in são sebastião (southeastern brazil). Natural Hazards Research https://doi.org/10.1016/j.nhres.2024.11.005 (2024).
- 48. Pourghasemi, H. R., Yansari, Z. T., Panagos, P. & Pradhan, B. Analysis and evaluation of landslide susceptibility: a review on articles published during 2005–2016 (periods of 2005–2012 and 2013–2016). *Arabian Journal of Geosciences* 11, 193. https://doi.org/10.1007/s12517-018-3531-5 (2018).
- Vaka, D. S., Yaragunda, V. R., Perdikou, S. & Papanicolaou, A. Insar integrated machine learning approach for landslide susceptibility mapping in california. Remote Sensing 16, https://doi.org/10.3390/rs16193574(2024).
- 50. P. L., C, M., Mathew, A. & Shekar, P. R. Machine learning and deep learning-based landslide susceptibility mapping using geospatial techniques in wayanad, kerala state, india. *HydroResearch* 8, 113–126, https://doi.org/10.1016/j.hydres.2024.10.001(2025).
- 51. Ercanoglu, M. & Gokceoglu, C. Use of fuzzy relations to produce landslide susceptibility map of a landslide prone area (west black sea region, turkey). Engineering Geology 75, 229–250. https://doi.org/10.1016/j.enggeo.2004.06.001 (2004).
- 52. Balamurugan, G., Ramesh, V. & Touthang, M. Landslide susceptibility zonation mapping using frequency ratio and fuzzy gamma operator models in part of nh-39, manipur, india. *Natural Hazards* 84, 465–488. https://doi.org/10.1007/s11069-016-2434-6 (2016).
- 53. Çellek, S. Effect of the slope angle and its classification on landslide. *Natural Hazards and Earth System Sciences Discussions* **2020**, 1–23. https://doi.org/10.5194/nhess-2020-87 (2020).
- 54. Empresa Paulista de Planejamento Metropolitano S.A. EMPLASA. Modelo Digital de Superfície (MDS) Ano: 2010 e 2011 Resolução Espacial: 5 metros Formato: Raster Abrangência: Estado de São Paulo (2010). [Digital Surface Model], http://www.metadados.idesp.sp.gov.br/catalogo/srv/por/catalog.search#/metadata/a3f7abc5-d134-43e9-a71f-3e21128d873b.
- 55. Cellek, S. The effect of aspect on landslide and its relationship with other parameters. In Zhang, Y. & Cheng, Q. (eds.) *Landslides*, chap. 2, https://doi.org/10.5772/intechopen.99389(IntechOpen, Rijeka, 2021).
- 56. Çellek, S. Morphological parameters causing landslides: A case study of elevation. *Bulletin of the Mineral Research and Exploration* **162**, 197–224. https://doi.org/10.19111/bulletinofmre.649758 (2020).
- 57. Peckham, S. D. Profile, plan and streamline curvature: A simple derivation and applications. In *Proceedings of Geomorphometry* (Redlands, CA, USA, 2011).
- 58. Kalantar, B. et al. Landslide susceptibility mapping: Machine and ensemble learning based on remote sensing big data. *Remote Sensing* 12, doi:10.3390/rs12111737 (2020).
- 59. San, B. T. An evaluation of svm using polygon-based random sampling in landslide susceptibility mapping: The candir catchment area (western antalya, turkey). *International Journal of Applied Earth Observation and Geoinformation* **26**, 399–412. https://doi.org/10.1016/j.jag.2013.09.010 (2014).
- 60. Kiss, R. Determination of drainage network in digital elevation model, utilities and limitations. *Journal of Hungarian Geomathematics* 2, 16–29 (2004).
- 61. Lee, C.-T. Re-evaluation of factors controlling landslides triggered by the 1999 chi–chi earthquake. In Ugai, K., Yagi, H. & Wakai, A. (eds.) Earthquake-Induced Landslides, 213–224 (Springer Berlin Heidelberg, Berlin, Heidelberg, 2013).
- 62. Panday, S. & Dong, J.-J. Topographical features of rainfall-triggered landslides in mon state, myanmar, august 2019: spatial distribution heterogeneity and uncommon large relative heights. *Landslides* 18, 3875–3889. https://doi.org/10.1007/s10346-02 1-01758-7 (2021).

- 63. Riley, S. J., DeGloria, S. D. & Elliot, R. Index that quantifies topographic heterogeneity. Intermountain Journal of sciences 5, 23-27
- 64. Trevisani, S., Teza, G. & Guth, P. L. Hacking the topographic ruggedness index. Geomorphology 439, 108838. https://doi.org/10.1 016/j.geomorph.2023.108838 (2023).
- 65. Beven, K. J. & Kirkby, M. J. A physically based, variable contributing area model of basin hydrology / un modèle à base physique de zone d'appel variable de l'hydrologie du bassin versant. Hydrological Sciences Bulletin 24, 43-69. https://doi.org/10.1080/0262
- 66. Kopecký, M., Macek, M. & Wild, J. Topographic wetness index calculation guidelines based on measured soil moisture and plant species composition. Science of The Total Environment 757, 143785. https://doi.org/10.1016/j.scitotenv.2020.143785 (2021).
- Cellek, S. Effect of stream distance on landslide. In SETSCI Conference Proceedings, vol. 4, pp268–275. ISAS2019 (SETSCI, Ankara, Turkey, 2019).
- 68. Nguyen, C. C. et al. Assessment of the Effects of Rainfall Frequency on Landslide Susceptibility Mapping Using AHP Method: A Case Study for a Mountainous Region in Central Vietnam, 87-98 (Springer International Publishing, Cham, 2023).
- 69. Brazilian Institute of Geography and Statistics. Mapa municipal estatístico. Map [Scale: 1:50.000] (2011). https://geoftp.ibge.gov. br/cartas_e_mapas/mapas_para_fins_de_levantamentos_estatisticos/censo_demografico_2010/mapas_municipais_estatisticos/ sp/sao_sebastiao_v2.pdf.
- 70. Haines-Young, R. Land use and biodiversity relationships. Land Use Policy 26, \$178-\$186. https://doi.org/10.1016/j.landusepol.2 009.08.009 (2009) (Land Use Futures.).
- 71. Carvalho, R. M. Classificação intraurbana da cobertura do solo com imagens do cbers-4a. In Anais do XXI Simpósio Brasileiro de Sensoriamento Remoto (Galoá, Salvador, BA, Brasil, 2025)
- 72. Henriques, C., Zêzere, J. L. & Marques, F. The role of the lithological setting on the landslide pattern and distribution. Engineering
- Geology 189, 17–31. https://doi.org/10.1016/j.enggeo.2015.01.025 (2015).
 73. Potekar, U. P., Naik, D. & Patil, A. S. Geospatial approach for landslide susceptibility mapping techniques: A case study of ratnagiri district, maharashtra, india. Disaster Advances 16, 34-45. https://doi.org/10.25303/1604da034045 (2023).
- 74. Geological Survey of Brazil. Carta de suscetibilidade a movimentos gravitacionais de massa e inundações: município de são sebastião - sp. Map [Scale: 1:25.000] (2017). https://rigeo.sgb.gov.br/handle/doc/23448.
- 75. Walker, J. & Awange, J. L. Relief and Vertical Sections, 31-54 (Springer International Publishing, Cham, 2018).
- 76. Zhang, B. et al. A geomorphological regionalization using the upscaled DEM: the beijing-tianjin-hebei area, china case study. Scientific Reports 10, 10532. https://doi.org/10.1038/s41598-020-66993-9 (2020).
- 77. Liu, Y., Deng, Z. & Wang, X. The effects of rainfall, soil type and slope on the processes and mechanisms of rainfall-induced shallow landslides. Applied Sciences 11, https://doi.org/10.3390/app112411652(2021).
- 78. Andriani, A., Rahmadani, T., Syuheri, B. T. & Syukur, M. Effect of physical environmental characteristics on landslide potential in kuranji watershed, padang-west sumatera. In E3S Web of Conferences, vol. 464, 02010 (EDP Sciences, 2023)
- 79. Guzzetti, F., Gariano, S. L., Peruccacci, S., Brunetti, M. T. & Melillo, M. Chapter 15 rainfall and landslide initiation. In Morbidelli, R. (ed.) Rainfall, 427-450, https://doi.org/10.1016/B978-0-12-822544-8.00012-3(Elsevier, 2022).
- 80. de Souza, D. C. et al. Extreme rainfall and landslides as a response to human-induced climate change: a case study at baixada santista, brazil, 2020. Natural Hazards 120, 10835-10860. https://doi.org/10.1007/s11069-024-06621-1 (2024).
- Dey, S., Das, S. & Saha, A. Exploring uncertainty analysis in gis-based landslide susceptibility mapping models using machine learning in the darjeeling himalayas. Earth Science Informatics 18, 42. https://doi.org/10.1007/s12145-024-01561-7 (2024).
- 82. Sistema Ambiental Paulista. Logradouros (2013). https://datageo.ambiente.sp.gov.br/serviceTranslator/rest/getXml/Geoserver_ WMS/Logradouros/1435844626817/wms
- 83. Wang, L. & Liu, H. An efficient method for identifying and filling surface depressions in digital elevation models for hydrologic analysis and modelling. International Journal of Geographical Information Science 20, 193-213. https://doi.org/10.1080/13658810 500433453 (2006).
- 84. Conrad, O. Tool basic terrain analysis (2005). https://saga-gis.sourceforge.io/saga_tool_doc/7.8.0/ta_compound_0.html.
- 85. Conrad, O. Tool terrain ruggedness index (tri) (2010). https://saga-gis.sourceforge.io/saga_tool_doc/7.6.1/ta_morphometry_16. html.
- 86. GDAL/OGR contributors. gdal proximity Generate raster proximity map (n.d.). Accessed: 2025-01-11.
- 87. Bonini, J. E., Martins, T. D., Sugiyama, M. T. D. O. & Vieira, B. C. Landslide inventory of the 2023 serra do mar disaster (brazil). Discover Geoscience 3, 40. https://doi.org/10.1007/s44288-025-00153-2 (2025).
- 88. RStudio Team. RStudio: Integrated Development Environment for R. Posit Software, PBC (2025). https://posit.co/download/rstud io-desktop/.
- 89. Saaty, T. L. Axiomatic foundation of the analytic hierarchy process. Management Science 32, 841-855 (1986). http://www.jstor.or g/stable/2631765
- 90. Saaty, T. L. How to make a decision: The analytic hierarchy process. European Journal of Operational Research 48, 9-26, https://d oi.org/10.1016/0377-2217(90)90057-I(1990). Desicion making by the analytic hierarchy process: Theory and applications, https: //www.sciencedirect.com/science/article/pii/037722179090057I.
- 91. Donegan, H. & Dodd, F. A note on saaty's random indexes. Mathematical and Computer Modelling 15, 135-137. https://doi.org/ 10.1016/0895-7177(91)90098-R (1991).
- 92. da Silva, S. E., Fávero, L. P., Ângelo Lellis Moreira, M. & dos Santos, M. Proposal of a diversified investment portfolio in stocks: An approach to ahp-gaussian method. Procedia Computer Science 221, 418-425, https://doi.org/10.1016/j.procs.2023.07.056(2023). h ttps://www.sciencedirect.com/science/article/pii/S1877050923007524.
- 93. de Moura Pereira, D. A. et al. Selection of agroindustry real estate funds, based on the ahp-gaussian, for an investment portfolio. Procedia Computer Science 221, 718-725, https://doi.org/10.1016/j.procs.2023.08.043(2023). https://www.sciencedirect.com/scie nce/article/pii/S1877050923008013
- 94. Bremm De Carvalho, E., Ângelo Lellis Moreira, M., Vilarinho Terra, A., Francisco Simões Gomes, C. & dos Santos, M. Proposal of criteria for selection of oil tank maintenance companies at transpetro through multimethodological approaches. In Ranganathan, G., Bestak, R. & Fernando, X. (eds.) Pervasive Computing and Social Networking, 521-531 (Springer Nature Singapore, Singapore, 2023).
- 95. Gavião, L. O., Lima, G. B. A., Garcia, P. A. d. A. & Teixeira, L. d. S. Decision support based on performance data using the analytic hierarchy process without expert judgement. Brazilian Journal of Operations & Production Management 21, 1882, https://doi.org /10.14488/BJOPM.1882.2024(2024).
- 96. Machado, G. d. O., Souza, H. F., Cabral, P. S. B., Limongi, R. & dos Santos, M. Ranking of artificial intelligence tools to assist in the writing of scientific articles using the gaussian ahp method. ARACÊ 7, 1039-1048, https://doi.org/10.56238/arev7n1-063(2025).
- 97. Bispo, P. d. C., Almeida, C. M. d., Valeriano, M. d. M., Medeiros, J. S. d. & Crepani, E. Análise da suscetibilidade aos movimentos de massa em são sebastião (sp) com o uso de métodos de inferência espacial. Geociências 30, 467-478 (2011). https://www.perio dicos.rc.biblioteca.unesp.br/index.php/geociencias/article/view/5563.
- Zêzere, J., Pereira, S., Melo, R., Oliveira, S. & Garcia, R. Mapping landslide susceptibility using data-driven methods. Science of The Total Environment 589, 250-267. https://doi.org/10.1016/j.scitotenv.2017.02.188 (2017).
- 99. Bravo-López, E., Fernández Del Castillo, T., Sellers, C. & Delgado-García, J. Landslide susceptibility mapping of landslides with artificial neural networks: Multi-approach analysis of backpropagation algorithm applying the neuralnet package in cuenca, ecuador. Remote Sensing 14, 3495. https://doi.org/10.3390/rs14143495 (2022).

- Google Maps; SIO; NOAA; U.S. Navy; NGA; GEBCO; Landsat/Copernicus. Satellite image from google maps. https://www.google.com/maps (2025). Accessed July 19, 2025.
- 101. Fagerland, M. W., Lydersen, S. & Laake, P. The mcnemar test for binary matched-pairs data: mid-p and asymptotic are better than exact conditional. *BMC Medical Research Methodology* 13, 91. https://doi.org/10.1186/1471-2288-13-91 (2013).
- 102. SAISP Sistema de Alerta de Inundações de São Paulo. São Paulo Weather Radar (Radar Meteorológico de São Paulo). https://www.saisp.br/estaticos/sitenovo/home.html (2024). Accessed: 2025-01-27.
- 103. Mantovani, J. R., Guimarães, Y. C. & Alcântara, E. H. d. From data to decision: Multi-criteria mapping of landslide susceptibility in são sebastião. In Anais do XXI Simpósio Brasileiro de Sensoriamento Remoto (Galoá, Salvador, 2025). Acesso em: 30 ago. 2025.
- 104. Colkesen, I., Sahin, E. K. & Kavzoglu, T. Susceptibility mapping of shallow landslides using kernel-based gaussian process, support vector machines and logistic regression. *Journal of African Earth Sciences* 118, 53–64 (2016).
- 105. Xie, W. et al. Landslide hazard assessment based on bayesian optimization-support vector machine in nanping city, china. *Natural Hazards* 109, 931–948 (2021).
- 106. Gao, Z. et al. Landslide risk assessment of high-mountain settlements using gaussian process classification combined with improved weight-based generalized objective function. *International Journal of Disaster Risk Reduction* 67, 102662 (2022).
- 107. Coelho, R. D., Viana, C. D., Lindsay, J. B. & Grohmann, C. H. Influence of data resolution on logistic regression models for landslide susceptibility in tropical environments. In *Proceedings of the 8th International Conference on Geomorphometry*. CNR IRPI and University of Perugia (International Society for Geomorphometry, Perugia, Italy, 2025). Acesso em: 30 ago. 2025.
- 108. Obara, T. S., Louro, V. H. A. & Antonelli, T. Mapeamento de risco em são sebastião e bertioga utilizando ferramentas de machine learning (2023).

Acknowledgements

This research was supported by the São Paulo Research Foundation (Nos. 24/02748-7, 21/11435-4, and 20/09215-3). National Council for Scientific and Technological Development (Nos. 311324/2021-5).

Author contributions

R. M. C. wrote the manuscript text, R.M. C, E. V. E. S., and R. P. Q. conducted the experiment, R. M. C., C. M. A, and A. C. P. L. F. C. analysed the results, M. S. developed the applied method, A. C. P. L. F. C. provided financial support. All authors reviewed the manuscript.

Funding

Open access funding provided by University of Vienna.

Declarations

Competing interests

The authors declare no competing interests.

Additional information

Supplementary Information The online version contains supplementary material available at https://doi.org/10.1038/s41598-025-22136-6.

Correspondence and requests for materials should be addressed to R.M.-C. or R.P.Q.

Reprints and permissions information is available at www.nature.com/reprints.

Publisher's note Springer Nature remains neutral with regard to jurisdictional claims in published maps and institutional affiliations.

Open Access This article is licensed under a Creative Commons Attribution-NonCommercial-NoDerivatives 4.0 International License, which permits any non-commercial use, sharing, distribution and reproduction in any medium or format, as long as you give appropriate credit to the original author(s) and the source, provide a link to the Creative Commons licence, and indicate if you modified the licensed material. You do not have permission under this licence to share adapted material derived from this article or parts of it. The images or other third party material in this article are included in the article's Creative Commons licence, unless indicated otherwise in a credit line to the material. If material is not included in the article's Creative Commons licence and your intended use is not permitted by statutory regulation or exceeds the permitted use, you will need to obtain permission directly from the copyright holder. To view a copy of this licence, visit https://creativecommons.org/licenses/by-nc-nd/4.0/.

© The Author(s) 2025